

POLITECNICO DI TORINO

Tesi di Laurea Magistrale

Ecological and Evolutionary Aspects of Microbial Population Growth in Confined Spaces

Author:

Víctor Peris Yagüe

Corso di Laurea Magistrale in Physics of Complex
Systems (International Track)

A.A. 2022/2023



**Politecnico
di Torino**



Supervisor: Dr. Alessandro Pelizzola (Politecnico di Torino)
External Co-Supervisor: Dr. Oskar Hallatschek (Universität Leipzig &
University of California Berkeley)
July 2023

Abstract

Spatial structure can play a pivotal role in defining an ecosystem's biodiversity, as well as its stability and adaptive capabilities. Emerging in the 1960s, a new theoretical framework was developed in the field of ecology aimed at describing island ecosystems [1], which quickly gained popularity and was applied to a wide range of ecosystems and even influenced policy-making [2]. Despite its impact, it largely remained a theoretical framework and many of its claims or hypotheses remained unverified experimentally [2, 3]. In fact, later work pointed to some of the gaps in island theory and stressed the need to couple ecological and evolutionary dynamics, as well as emphasizing the relevance of the correct choice of scale in describing ecosystems [3]. More recently, studies have emerged in the field of microbial ecology and evolution with an explicit focus on the effects of spatial structure [4]. Still, many open questions remain regarding eco-evolutionary dynamics in systems with a strong spatial dependence. In this work, we study a microbial ecosystem at the micro-scale consisting of an elongated cavity with one open and one closed end, whose tight spatial constraints confer it with very particular ecological properties. We generalize the study of Karita *et al.* [5] of these microbial communities by extending the study of a scale-dependent transition from a gaseous to a jammed state for the case of non-exponential microbial growth, in particular under the influence of resource depletion and an Allee-type cooperation. We also developed a novel, individual-based model based on the distinction between self-diffusion and collective diffusion. In particular, we use the model to study the stability of band-like structures and the takeover of cavities by strains with a high selective advantage, and we point to the presence of pinning impurities as band stabilizers in cavities, showing good agreement between the predictions of the simulations and experimental results. We also analyze Clone Size Distributions (CSD) in both jammed and

gaseous cavities, uncovering fundamental differences in the dynamics leading up to them and showing how the jammed state of larger cavities leads to lower diversity than the gaseous state, in direct contrast with island theory. Lastly, we discuss a novel mechanism, Invader-Sustained Jamming (ISJ), by which an invading strain can stabilize the resident population of a cavity into a jammed state without itself being able to take over the system, even for large selection advantages. Our results support the view that the properties of ecosystems can be highly sensitive to scale or spatial structure, especially close to transitions like the one between gas and jamming. In particular, the transition to jamming points to a tradeoff between stability and adaptation, as it leads to stabler populations and increased levels of resistance against invasion at the expense of a lower speed of adaptation.

Acknowledgments

First and foremost, I would like to thank Oskar for his openness to have me in the group, for always being available for guidance and discussions, for giving me such a wonderful project and for always being so friendly. Thank you as well to all the members of the lab, to Aditya, Joao, Birgit, Christian, Giulio and, in particular, to Valentin for all of the discussions we had together. Thanks to Yuya Karita as well for providing us with the experimental data that made it possible to validate some of the results of the thesis. Thank you as well to Prof. Alessandro Pelizzola for his role as supervisor from Politecnico di Torino. I also need to thank the people working at the Delegation of the Spanish Government in Barcelona, the workers of the Catalan Palace of Justice and the public servants of the Italian Consulate of Barcelona, for fighting against all odds to complete the administration procedure that allows me to graduate. Lastly, thank you to all friends here in Leipzig.

Contents

1	Introduction	7
1.1	Island Biogeography	7
1.2	Cavity Systems	11
1.3	Outline of the thesis	14
2	One-Dimensional Model	16
2.1	1D Reaction-Diffusion system	17
2.2	Newtonian analogy	19
2.3	Non-exponential population growth	25
2.4	Non-zero boundary conditions	31
3	Two-Dimensional Models	35
3.1	Soft-Disk Model	36
3.2	The two-diffusivities model	38
3.2.1	Self-diffusion <i>vs.</i> collective diffusion	39
3.2.2	The model	41
3.3	RD System with mixing	45
4	Strain Coexistence in cave-like Environments	48

4.1	Jammed vs. Gaseous caves	49
4.2	Bands in a jammed cave	50
4.2.1	Coexistence in the neutral case	50
4.2.2	Selection effects: logistic takeover	52
4.3	Stabilization of bands by pinning	58
4.4	Comparison with experiments	62
4.4.1	Pinning in experimental cavities	66
4.4.2	Jamming wave	66
4.4.3	Final remarks on Logistic takeover	68
5	Population Distributions in Cave-like Environments	71
5.1	Clone-Size Distribution	72
5.1.1	Jammed cavities	73
5.1.2	Gas Cavities	75
6	Invasion and Fixation in Cave-like Environments	85
6.1	Outsider-Induced Population	86
6.2	Invader-Sustained Jamming	87
7	Discussion	90
A	Appendix	99
A.1	Establishment length	99
A.2	Inter-band boundary under pinning.	100
A.3	Well-mixed approach to the CSD	101

Chapter 1

Introduction

1.1 The theory of island biogeography.

In 1967, Robert MacArthur and Edward Wilson published the book *The theory of island biogeography*[1]. In it, they emphasized the relevance of island ecosystems in developing a theory of the laws of ecology and evolution. After all, islands are well-defined spaces, with a numerable number of species and a certain level of isolation that makes their interactions with other ecosystems simpler than for continental ecosystems. Furthermore, MacArthur and Wilson argued that the great diversity in island size, geographical position, climate or isolation turns islands into effective replications of natural experiments, upon which a potential theory of biogeography could be tested [1]. On top of that, systems of islands (archipelagos) are a convenient starting point for the study of metapopulations and the role of migration between ecosystems.

Although MacArthur and Wilson first presented their ideas in the context of literal islands, they argued that the concept of ecological “island” extends beyond the literal patch of land in the sea. Any ecosystem that is well-defined in space, of a relatively small size, working mostly in isolation from other systems but with a certain degree of connectivity to them, can be understood as an ecological “island”. Particular examples include studies on single plants, caves, natural reserves, lakes, ponds or mountain tops [1, 2].

One of the main ideas proposed by MacArthur and Wilson is that the diversity of species in an island is proportional to the island area following a power law:

$$S = C \cdot A^z \quad (1.1)$$

where S is the number of species, A the area of the island, C some biogeography-dependent parameter, and $z > 0$ some scaling parameter (the number of species grows as the area of the island grows). Figure 1.1 shows this relation as presented in the original book by MacArthur and Wilson, for islands in the Caribbean. This is a priori a sensible idea: a larger ecosystem might allow for more ecological niches and thus lead to a larger number of potential species.

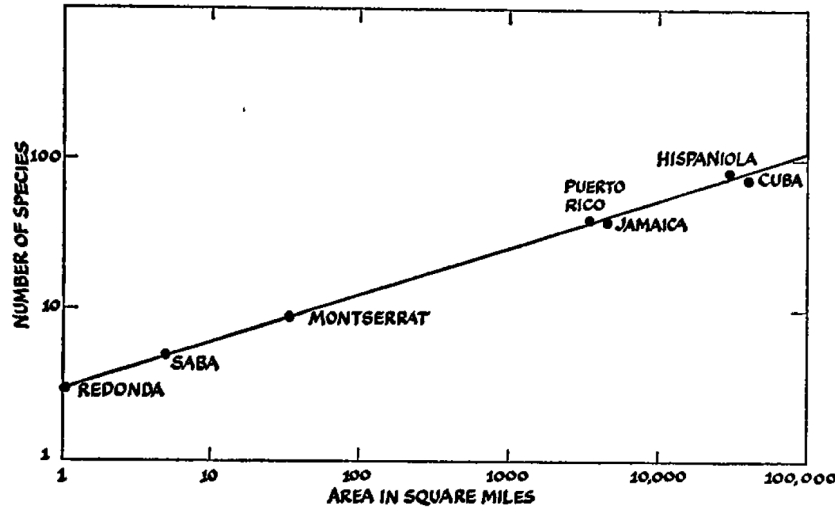


Figure 1.1: Relation between island area and number of species in islands in the Caribbean. Plot taken from the original publication by MacArthur and Wilson [1].

Another key idea by MacArthur and Wilson was that the number of species present in an island ecosystem is determined by a dynamical equilibrium between immigration and extinction rates in the island (see Figure 1.2.A). The argument proposed is as follows: if the number of species in an island grows then the rate of immigration of new species must decrease, as the potential for unfilled ecological niches, as well as the resources available

in the island, decrease and as new immigrants are likely to be of an already-present species. Conversely, as the number of species grows, so does the rate of extinction, simply because there are more species that can go extinct and because, for an island of a given area, a bigger total number of species must imply a lower number of individuals per species, making extinction events more likely.

Equally, MacArthur and Wilson postulated that the inter-island distances are inversely correlated with immigration rates, that is, that if an island is closer to some source region of individuals, then the rate of arrival of new species is larger. On the other hand, they argued that the extinction rate in islands is inversely proportional to the island area. If an island is smaller then, for a given number of species, one might expect inter-species interactions to be stronger (everyone is living closer together) leading to more extinction events. Both arguments are illustrated in Figure 1.2.B.

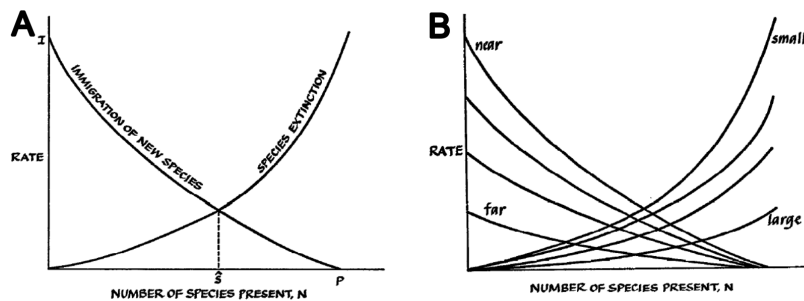


Figure 1.2: Idea of dynamic equilibrium in island ecosystems, as presented by MacArthur and Wilson [1]. **A)** Dynamic equilibrium. The crossing point between the extinction rate and the immigration rate of species in an island sets the steady-state number of species in it. The extinction rate is directly proportional and the immigration rate is inversely proportional to the number of species in the island. **B)** An increase in distance from the immigration source reduces the immigration rate of species (decreasing curves). A decrease in island area increases the rate of extinction events (increasing curves).

After MacArthur and Wilson published their book, their ideas gained popularity in the study of ecosystems and they were also readily applied by policy makers in the design of nature reserves [6]. In particular, the idea that the size of an ecosystem patch or island is proportional to its number of

species led to the idea that a large reserve is better than a small one, as well as that a single large reserve would be better than several small ones, for a given total area [2].

Despite their novelty and potential, MacArthur's and Wilson's ideas were not without criticism [6–8]. Their considerations and assumptions were considered too simplistic and heavily criticized by conservation biologists [8], as well as being generally far removed from real ecosystem dynamics [2, 8] and being intrinsically difficult to test experimentally. For instance, determining experimentally the number of species present in an ecosystem is heavily dependent on the method used and there is a large potential for undersampling.

In his seminal paper, *The problem of pattern and scale in ecology* [3], biologist Simon Levin expanded on the ideas of MacArthur and Wilson and argued about the importance of choosing the right scale when studying ecosystems, in particular if one is to produce the kind of predictive models necessary in ecosystem management [3]. MacArthur and Wilson had presented their theory in the highly specific context of islands and mostly for vertebrate species (amphibians, reptiles, fish and birds), but there was no basis to think that it might apply to these classes in different contexts or to species in larger/smaller ecosystems. Levin argued that understanding ecosystems requires an understanding of the underlying processes that occur at each scale, as well as how the mechanisms at one scale produce effects at different scales. In particular, Levin argued that the patchy (or island-like nature) of ecosystems holds at different scales, and he advocated for a thorough study of both the intra-island and inter-island dynamics for a full understanding of an ecosystem [3]. Levin also argued that the correct study of ecosystems must involve the coupling of ecological and evolutionary dynamics, something that was mostly omitted in MacArthur and Wilson's ideas.

The world of microbial populations is a potential test bed for all of the previous discussions. In microbial communities, ecological and evolutionary timescales can be comparable and experiments can be made in controlled environments. They might thus enable to test the ideas of MacArthur and Wilson in a quantitative manner. Additionally, in recent years, there has been a surge in studies highlighting the importance of spatial structure in microbial systems [4, 9–12]. After all, MacArthur and Wilson's ideas neglect the presence of spatial structure in ecological islands, but it is reasonable to expect that a certain degree of spatial organization will affect the eco-

evolutionary dynamics of an ecosystem.

In this thesis, we shall explore the properties of a particular type of microbial system at the micrometer scale, that of cavity-like environments. We will discuss how some of their properties compare with the island theory that we discussed here (in cavities diversity will be measured in strains or lineages, not species), but they will also uncover other novel phenomena not directly related to island theory that we will discuss in much more detail. In the next sections we present the paper on which this thesis is based, that of Yuya Karita and coauthors [5]. In particular, in Section 1.2 we will present in more detail the cavity environment, as well as the experiments performed in [5], which will serve as a starting point for the rest of the thesis.

1.2 Cavities and the panflute experiment

We can intuitively understand a cavity as a confined, mostly elongated space, closed at one end but open at the other, where the cavity connects to some outer world. Cavity-like environments are found in nature in a variety of systems, including skin follicles and pores [13, 14] or intestinal crypts (see Figure 1.3) [15, 16]. Cavities can easily be understood as islands in the MacArthur-Wilson sense. They are environments in a well-defined position, capable of sustaining a population within and which find themselves inside a larger environment, allowing for migration into the cavity from any other cavity or, more generally, from the larger environment outside the cavity (e.g.: the lumen in the gut for a crypt or the air for a skin follicle). One very particular aspect of this kind of cavities is their size: skin pores are about $60\ \mu\text{m}$ in diameter [17], and intestinal crypts in humans are about $50 - 70\ \mu\text{m}$ in diameter [18]. For typical bacterial sizes of about $1\ \mu\text{m}$, we can easily get a grasp of just how tight these environments are: the amount of individuals living in any given section of the cavity will typically be of a few tens, at most a few hundreds. We might thus naturally expect that stochasticity plays an important role and that spatial structure will be key to understanding their population dynamics.

In 2022, Karita and coauthors published a paper in which they set out to study these kind of cavity systems using the bacterium *A. Indionesiensis* [5]. In their study, they devised the following experimental setup: a long channel

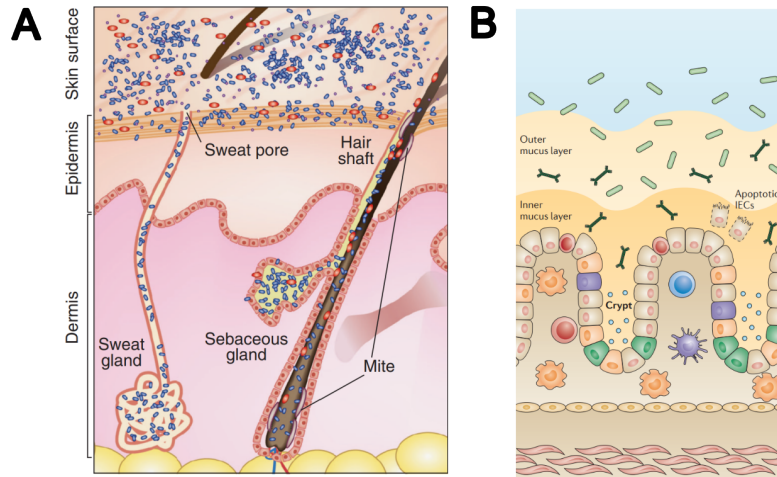


Figure 1.3: Examples of cavity-like environments in natural systems. **A)** Skin follicles and pores. Taken from Kong&Segre, 2012 [13]. **B)** Small crypts in the intestinal tract. Taken from Mowat&Agace, 2014 [16].

allows for the flow of fluid with nutrients and cells. Cavities of varying length protrude from this channel, thus producing a setup that looks like a panflute (see Figure 1.4). Cells are non-motile, they move passively by diffusion, and they can enter the cavities and have the potential of colonizing them through proliferation. In their experiments, the authors found that there are two major transitions in the cavities. When a cavity is too short, diffusion is too strong and the outwash of cells dominates proliferation, making impossible the stable establishment of a bacterial colony inside a cavity (see cavity 1 in Figure 1.4). If the cavity is long enough, then proliferation dominates and the cavity can be colonized. The second transition occurs at a larger cavity length. If a cavity is shorter than the critical length, then the population in the cavity appears to be in a gaseous state with a high diffusion of individual cells (see cavities 2-6 in Figure 1.4). If it is longer, then proliferation is too large compared with the diffusion-driven outwash and the population appears to be in a jammed state: cells have a very low self-diffusion, the crowding limits their movement and they are essentially stuck in place by the presence of neighboring cells (see cavities 7-8 in Figure 1.4). The authors actually developed a theoretical reaction-diffusion model that predicts this kind of transition in a one-dimensional cavity [5]. We shall go deeper into it in Chapter 2 of the thesis, as we will use it throughout the thesis and its

extension will lead to some new results.

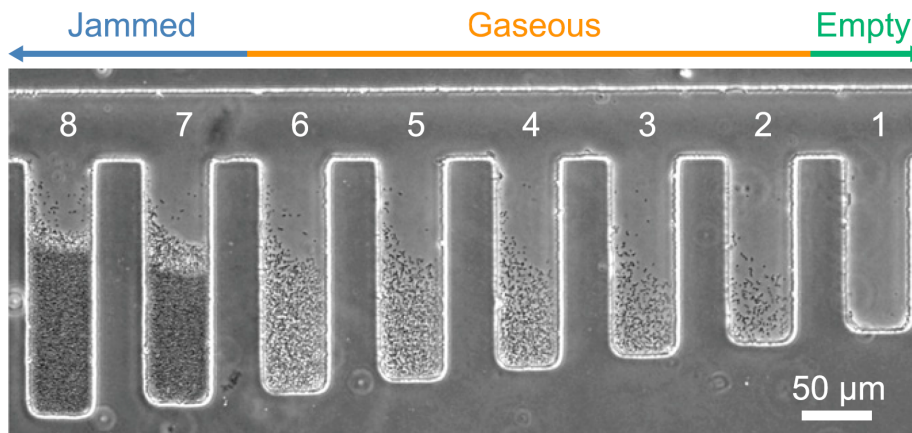


Figure 1.4: *Image taken from Karita et al., 2022 [5].* Experimental panflute device. Cells and nutrients flow in the top channel, and cavities of different lengths emanate from it. The length of the cavities determines whether cells can colonize them or not: cavity 1 is too short and can only sustain an empty steady state, cavities 2-6 can sustain a gaseous population, and cavities 7-8 are long enough that the population of cells jams.

The results of this study already support Levin’s claim that the correct choice of scale is paramount in the study of an ecosystem. A change of less than doubling the length of a cavity covers all three possible states of the population (empty, gas and jammed) and the change from gaseous to jammed is discontinuous and occurs for a change in cavity length of less than 5% [5].

A second result from the study is that populations in the jammed state are very resistant to invasion, even against much-fitter invaders. To show this, the authors in [5] introduced an antibiotic into the panflutes that reduced the growth rate of the resident bacteria. This causes the jamming threshold to move towards longer cavity lengths, unjamming some populations and “gasifying” them. The authors then introduced an antibiotic-resistant bacterial strain. The resistant strain, despite holding a big selection advantage over the resident strain, was able to invade only gaseous cavities. Figure 1.5 shows this process. In their discussion, the authors argue that the inability of the fitter strain to invade is due to the inherent mechanical advantage of the resident strain in the jammed state: the authors postulate that the dynamics

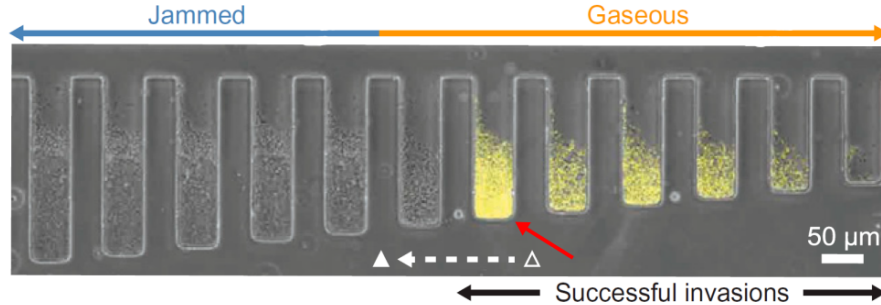


Figure 1.5: *Modified from [5].* Invasion in cavities. Antibiotic is introduced in cavities, reducing the growth rate of the resident strain (grey). An antibiotic-resistant strain (yellow) is then introduced into the cavity. Its selective advantage allows it to invade gaseous cavities, but jammed cavities remain immune to jamming. The unfilled triangle marks the transition from gaseous to jamming in the absence of antibiotic, and the filled triangle marks the same in presence of antibiotic. Notice in the cavity marked with a red arrow, how once the invader strain has taken over the cavity, its larger growth rate causes it to re-jam the cavity.

in a jammed cavity must be dominated by a small number of cells at the floor (the closed end) of the cavity. A successful invading cell would then first have to make its way to the floor in order to take over the cavity, an occurrence that is practically impossible if the resident population is jammed. Jamming can thus act as a stabilizing factor in cavity-like environments, a factor that could help explain the high stability of some bacterial populations in the gut or the skin despite their overall low numbers and the large fluctuations in the environment around them [5, 19, 20].

1.3 Outline of the thesis

The previous discussions elucidate how the study of cavity environments can uncover novel phenomena, and that they can be used to quantitatively test the feasibility of some of the ideas about “island” ecosystems. In this thesis, we shall further the study of cavity environments, progressing in the understanding of the different phases of the populations within, the transitions

between them, and the ecological and evolutionary dynamics of the cells living within.

Chapter 2 will be devoted to the 1D reaction diffusion system used by Karita *et al.* [5]. We will reproduce some of the results from their study and extend the model to study the effects of non-exponential growth on the gas-jam transition. We will also probe the effects of different boundary conditions on the system, which will uncover a new type of cooperation: Invader-Sustained Jamming (ISJ). In Chapter 3, we will present different models that allow the study of cell populations in cavities with individual-cell resolution. Particular emphasis is placed on a new, individual-based model that pivots on the distinction between self-diffusion and collective-diffusion, which will be used in subsequent chapters to study population dynamics inside the cavities. In Chapter 4, we will study the coexistence of strains in cavities. In particular, we will focus on the coexistence of band-like structures arising in jammed cavities, as first discovered in [5], and we will explore competition quantitatively, probing some of our new theoretical predictions with actual experimental data. In Chapter 5 we will study the diversity of populations in cavities, in particular by looking at Clone Size Distributions (CSDs) in both gaseous and jammed cavities. Lastly, in Chapter 6, we will study in more detail the cooperation phenomenon of ISJ introduced in Chapter 2. Chapter 7 will be devoted to a deeper discussion on the results found throughout the thesis, a reflection on how they relate back to the theory of island biogeography, as well as potential limitations and appealing directions of future research.

Chapter 2

One-Dimensional Model

By far the simplest approach to modeling a cavity-like environment is to reduce it to a single dimension. Doing so allows one to obtain results, both analytical and numerical, in a short time and to gain some intuition on the dynamics of cell colony growth in cavities. Even though the power of such simple models is obviously limited, they predict some very interesting phenomena and give quantitative predictions that agree with much more complex models. In this chapter, we will first motivate and present a one-dimensional model used to explain the experimental results in [5]. We will recover some of the results from that paper and extend the analytical study to arrive to the first novel results in the thesis. In particular, we will see that the 1D model correctly predicts a transition from a gas state to a jammed state in the density profile inside the cavity, as well as a possible involuntary cooperation mechanism that confers a colony inside a cavity with some colonization resistance against invasions.

2.1 1D Reaction-Diffusion system

The elongated nature of a cavity makes the one-dimension assumption reasonable, resting on two major assumptions. The first is that the observables that describe the population, in particular the cell density, only change along the length of the cave. The second is that the same must be true of any outside forces acting on the cell population, namely how the motion of the fluid inside the cavity carries cells with it. The second assumption can be completely overlooked if one ignores the effect of advection altogether, which is reasonable for some real systems under experimental conditions, whenever the population grows far enough away from the mouth of the cave to be unaffected by the flow from the fluid coming in from the main channel [5].

The simplest one-dimensional model rests on treating the cell population as a continuous medium, characterized by the density of cells, ρ , in cells per unit length. The dynamics of the microbes in a cavity of length L are thus given by the following reaction-diffusion equation

$$\begin{aligned}\partial_t \rho(y, t) &= -\partial_y(j(y, t)) + b(\rho(y, t)) \\ j(y, t) &= -D(\rho)\partial_y \rho(y, t)\end{aligned}\tag{2.1}$$

corresponding to Fick's 2nd Law with a birth term, $b(\rho(y, t))$, due to cell growth, where $j(y, t)$ is the current of density given by Fick's 1st Law, $D(\rho(y, t))$ is the diffusivity, which is in general a function of the density, t is the time variable and y the position from the floor of the cavity. In the discussions that follow, we will simplify the notation $\rho(y, t)$ to ρ for brevity, making the dependence on space and time explicit only when necessary. Note that the dependence of the diffusivity D on the density ρ will be crucial to understand the behavior of the gas and jammed states, something that will be discussed in much more detail in Section 2.2.

Equation 2.1 is solved with the following boundary conditions:

$$\begin{aligned}j(0, t) &= 0, \quad \forall t \\ \rho(L, t) &= \rho_L, \quad \forall t\end{aligned}\tag{2.2}$$

corresponding to zero-flux at the floor of the cavity and a fixed density value at the mouth of the cavity, respectively. The first boundary condition is motivated by the fact that cells cannot cross the cavity wall at the floor.

The second stems from the fact that the density of cells in the main channel from which the cavity protrudes is kept more or less constant. In particular, we will work with the condition $\rho_L = 0$, corresponding to a channel which is, for all practical purposes, empty. This condition will be relaxed in Section 2.4, giving rise to an interesting type of cooperation effect.

In the rest of this section and all of the following section, we will work with a birth term of the type

$$b(\rho) = b \cdot \rho \quad (2.3)$$

where b is the growth rate of the microbes in units of $1/t$. This implies that microbes in the system always grow exponentially, a very strong assumption but which is compatible with the experimental results from [5]. In section 2.3 we will relax this condition and explore the effects of different kinds of microbial growth.

Figure 2.1 shows an illustration of a cavity and a typical density profile in the gaseous phase, under the simplification to one dimension.

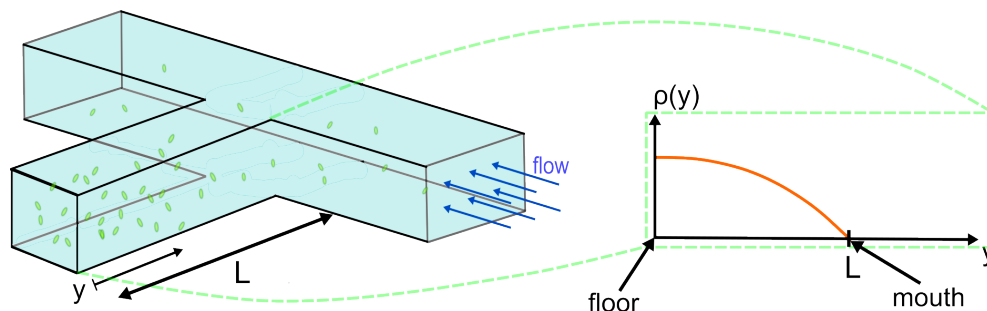


Figure 2.1: Left: Example of a cavity in a panflute setup. The panflute has a main channel where fluid with cells and nutrient flows. Cavities stem out of the main channel and microbes can accumulate in them and proliferate, forming colonies and accumulating near the bottom of the . Right: Illustration of the cell density profile under the simplification to one dimension. The density satisfies the no-flux condition at the floor and can be assumed to be 0 at the mouth, since the number of cells in the main channel is very low.

The system presented in Equations 2.1, 2.2 and 2.3 has a steady state that undergoes two transitions. The first one is the establishment transition. For cavity lengths under some establishment length L_{est} , the cavity cannot

sustain a stable steady state population, and the only stable solution to the system is $\rho = 0$ everywhere in the cavity (see Figure 2.2). If, instead, the length of the cavity is such that $L > L_{est}$, the cavity is able to sustain a non-zero population. It can be shown using linear stability analysis (see Appendix A.1 for a detailed derivation, taken from [5]) that the transition occurs at the establishment length:

$$L_{est} = \frac{\pi}{2} \sqrt{\frac{D_0}{b}} \quad (2.4)$$

where $D_0 \equiv D(0)$ is the value of the diffusivity at zero cell density.

For values of L slightly above the establishment length, and as long as the diffusivity increases sufficiently with ρ , the cavity supports a stable microbial population in what we shall call a *gas* or *gaseous* state, characterized by a low cell density and in which the density profile is cosine-shaped (see Figure 2.2), in agreement with experiments [5].

At some other critical length, $L^* > L_{est}$, the system undergoes a second transition from the gas-like state into a jammed state in which the density of cells is really high and the profile looks almost flat near the floor of the cavity and is then gas-like near the mouth (see Figure 2.2). The jammed phase occurs when the cell density is increased above some jamming threshold, ρ_{jam} , at which points the cells are in physical contact with each other and movement in the cavity comes mostly not from Brownian motion but from excluded-volume repulsion between cells [5].

In the next section, we shall discuss in detail an analogy to a Newtonian problem that can be used to derive the steady-state value of the density at the floor of the cavity from Equation 2.1. This will be useful to discuss in more detail the establishment and jamming transitions presented in this section.

2.2 Newtonian analogy

In steady state, Equation 2.1 can be easily rewritten as

$$0 = \partial_y \left(D(\rho) \partial_y \rho(y) \right) + b \cdot \rho(y) \quad (2.5)$$

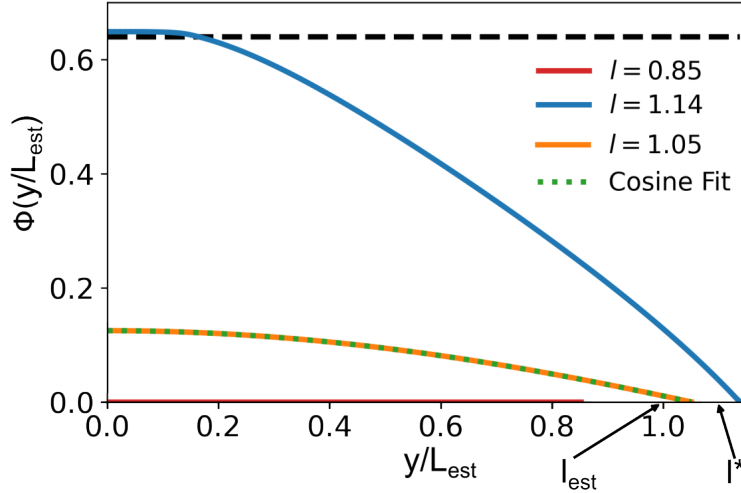


Figure 2.2: Simulated packing-fraction profiles using the 1D reaction-diffusion system for different reduced lengths, $l = L/L_{est}$, obtained by varying the actual length of the cavity. For $l < l_{est} \equiv 1$, the steady state solution is an empty cave (red). For $l_{est} < l < l^*$, the profile is typical of a population in a gaseous state (orange) [5] and can be well-approximated by a cosine profile (dotted green line). For $l > l^*$, the population enters the jammed phase, with a flat profile saturated around the jamming packing fraction (dotted black line) close to the floor and a gas-like phase closer to the mouth of the cavity (blue).

where the density profile is now independent of time.

Now consider a basic one-dimensional Newtonian problem of the type

$$\ddot{x} = -\partial_x U(x) \quad (2.6)$$

representing an object of unitary mass falling due to some potential $U(x)$, where x is the particle's position with zero initial velocity. If the particle moves from an initial position x_0 , conservation of energy implies that

$$U(x_0) - U(x(t)) = \frac{1}{2}v(x(t))^2 \quad (2.7)$$

where $v(x(t))$ is the velocity of the particle in position $x(t)$ at time t . The total time, T , taken for the particle to reach some final position x_f , $x_f > x_0$,

is thus

$$T = \int_0^T dt = \int_{x_0}^{x_f} \frac{1}{v} dx = \int_{x_0}^{x_f} \frac{1}{\sqrt{2(U(x_0) - U(x))}} dx \quad (2.8)$$

and it can be easily calculated by computing the integral analytically or numerically. If $x_f < x_0$, then Equation 2.8 has a negative sign or, equivalently, the limits of integration are exchanged; this small correction simply comes from the ambiguity in the sign of the velocity that results from Equation 2.7.

It turns out that, as shown by Yuya Karita *et al.* in [5], it is possible to recast Equation 2.5 into a Newtonian equation like Equation 2.6 where the position y plays the role of time, such that the total length of the cavity is akin to T and can be calculated using Equation 2.8.

This can be done by introducing the following variable

$$\Pi(\rho) = \int_0^\rho D(\rho') d\rho' \quad (2.9)$$

and the potential

$$\begin{aligned} U(\Pi(\rho)) &= \int_0^{\Pi(\rho)} b(\rho(\Pi')) d\Pi' \\ &= \int_0^\rho b(\rho') D(\rho') d\rho' \\ &\equiv U(\rho) \end{aligned} \quad (2.10)$$

such that we are left with the equation

$$\partial_y^2 \Pi = -\partial_\Pi U(\Pi) \quad (2.11)$$

which is evidently like Equation 2.6 with y taking the role of time.

Then, using Equation 2.8, the length of the cavity can be calculated as

$$L = \int_{\rho(L)=0}^{\rho(y=0)=\rho_0} \frac{D(\rho)}{\sqrt{2(U(\rho_0) - U(\rho))}} d\rho \quad (2.12)$$

Before we proceed to the evaluation of Equation 2.12, it is important to discuss two elements: the distinction between density and packing fraction, and the form of $D(\rho)$.

The packing fraction, Φ , is the ratio between the area/volume occupied by the cells and the area/volume of the space that they live in, in two/three dimensions, respectively. For a given cell density (in number of cells per unit area/volume), the conversion between density and packing fraction is simply

$$\begin{aligned}\rho &= \Phi \cdot A, & \text{in } 2D \\ \rho &= \Phi \cdot V, & \text{in } 3D\end{aligned}\tag{2.13}$$

where A/V is the area/volume of a single cell. ρ and Φ can be used indistinguishably for most practical purposes. The jammed state is more naturally described in terms of the packing fraction, since it is the physical limit to how closely-packed the cells can be, and it is independent of the area/volume of a single cell. On the other hand, when talking about cell populations in a cavity, it is more natural to speak about cell density. In this manuscript both terms shall be used indistinguishably (and the same is true about their symbols), but with some general trend: the rest of this first chapter will see a heavier use of the term “packing fraction”, whereas in all the chapters that follow we shall talk almost exclusively about “density”.

Regarding the diffusivity function, in the entirety of this manuscript we shall use the diffusivity of hard spheres in three dimensions as in [5], stemming from the equation of state for hard spheres as given by the Carnahan-Starling (CS) Equation [21] (see Figure 2.3). This is only done for consistency and to facilitate the comparison with known results from [5], but the results presented in this thesis should not heavily depend on the exact shape of the function as long as it has the following two main traits: a positive slope in the region near zero packing fraction, followed by a strong enough negative slope in the regions of high packing fraction. This shape is what confers it the ability to stabilize a gaseous population at low packing fractions, as well as yielding the fold-bifurcation that gives rise to the gas-jam transition [5]. A second point to be made about the diffusivity function is its behavior above the jamming threshold when trying to solve the reaction diffusion system in Equation 2.1 by numerical integration. Ideally, wherever the system is in the jammed state the diffusivity is infinite (i.e.: a cell would respond immediately to a change in density caused by the movement or growth of cells around it), or at least orders of magnitude higher than in the gas state. One way to implement this behavior approximately in a numerical simulation is by adding a linear, strongly growing, term to the diffusivity for values above the jamming threshold, such that it mimics the expected behavior without losing

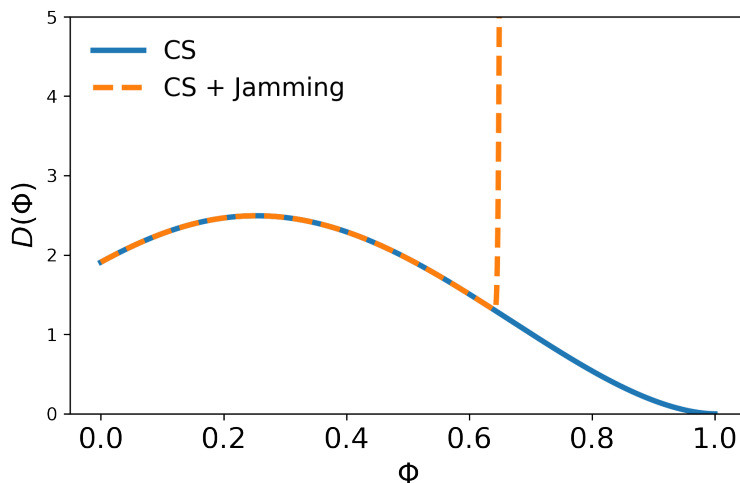


Figure 2.3: Diffusivity function for hard spheres from the Carnahan-Starling Equation (blue), with a correction to account for the transition to the jamming phase (orange). The positive slope for low packing fractions (Φ) allows the stabilization of a gaseous phase, while the negative slope at higher packing fractions promotes the transition to jamming.

numerical stability. The resulting diffusivity function is shown in Figure 2.3.

Going back to Equation 2.12, by evaluating it at different values of ρ_0 , we can construct a bifurcation diagram for the one-dimensional model which tells us what is the packing fraction at the floor of the cave, Φ_0 , as a function of the length of the cave, L . The resulting bifurcation diagram is shown in Figure 2.4. For lengths below the establishment length, the only stable solution is the empty state. For lengths above some critical value L^* , the empty state is unstable and the density grows until the packing fraction hits its maximum allowed value, corresponding to the jamming transition (in this case we use the value for random close packing of hard spheres, $\Phi_{jam} \approx 0.64$ [22], but once again, the general dynamics observed in the models used in this thesis should not heavily depend on its exact value).

Let us consider the reduced length

$$l = \frac{L}{L_{est}} = \frac{2L}{\pi} \sqrt{\frac{b}{D_0}} \quad (2.14)$$

such that $l_{est} = L_{est}/L_{est} \equiv 1$. For reduced lengths between l_{est} and l^* (corresponding to L^* at the jamming transition), the resulting curve from Equation 2.12 shows that it is possible to have a steady state population in a gas phase (see the curve of positive slope between $l = l_{est} = 1$ and the saddle-node bifurcation in Figure 2.4).

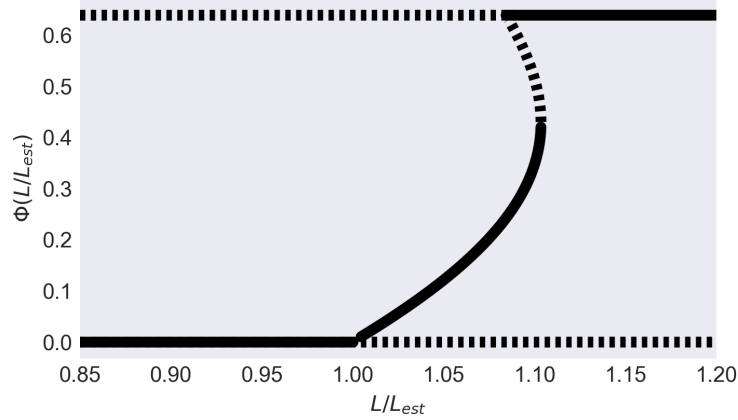


Figure 2.4: Bifurcation diagram for the packing fraction, Φ_0 , at the floor of the cavity as a function of its reduced length, $l = L/L_{est}$. Solid/dashed curves indicate stable/unstable fixed points, respectively. Φ_0 can be used as a measure of the state of the population: if $\Phi_0 = 0$ the cavity is empty, if $\Phi_0 = \Phi_{jam}$ the population is jammed and if $\Phi \in (0, \Phi_{jam})$ the population is in a gaseous state.

From the bifurcation diagram in Figure 2.4, we can see that the system allows for hysteresis. There is a region of bistability between l_{est} and l^* where the steady state can either be gaseous or jammed, depending on its history. If the system comes from low l , it stays in the gas state. If l keeps increasing, at some point it encounters the fold bifurcation at l^* and jumps to the jammed state. If l is then reduced, the system will stay in the jammed state until some lower threshold is reached, at which point it jumps down again to a gaseous state. Note that it makes sense to speak about time-changing reduced lengths because the reduced length l depends not only on the length of the cavity, but also on the diffusivity and the cell birth rate. Its change in time can thus be achieved via alterations to the birth rate, for instance through the use of antibiotics [5]. The ability of the system to

present hysteresis was numerically tested, with results being represented by the colored dots in Figure 2.5.

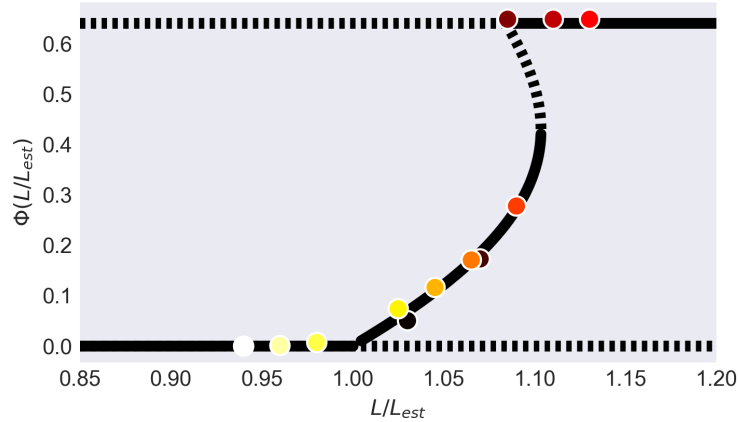


Figure 2.5: Bifurcation diagram as in Figure 2.4, with the results from the hysteresis test shown as dots. The test was performed by numerically integrating Equation 2.1 until a stable state was reached, then varying the reduced length of the system and repeating the process. The order of the simulations is given by the color of the dots: from fairest to darkest. Here, bistability is shown for $l = L/L_{est} \approx 1.09$. The system can be in a stable gas phase, if one comes from smaller l (light red), or a stable jammed phase, if coming from a l corresponding to a jammed state (dark red).

This section served to introduce the tools necessary to quantitatively predict the steady state of the microbial population in the cavity. The results presented in this section reproduce those found in [5] and are useful to give some intuitive understanding as to what happens in these cavity environments. In the next two sections, we shall use the tools presented here to find novel results, some of which have interesting ecological and evolutionary consequences.

2.3 Non-exponential population growth

In the previous two sections, we assumed that the birth rate of the cells in the system was a constant (see Equation 2.3). It is natural to ask what happens

if that assumption is lifted. Two phenomena stand out as prime candidates for this extension and they are the ones that we will consider: logistic growth and the Allee effect.

Logistic growth is the typical kind of growth experienced by populations whose environment supports a limited number of individuals. It is typical of microbial populations [23], but has even found use (and was actually first introduced to describe) human population growth [24]. Under logistic growth, a population $N(t)$ grows in time according to the differential equation

$$\partial_t N(t) = b_l(N) \cdot N = b\left(1 - \frac{N}{K}\right)N \quad (2.15)$$

where $b_l(N)$ is the growth rate of the system, given by b , the exponential growth rate, and K , the carrying capacity of the system. A population following logistic growth will saturate at its carrying capacity, with a growth rate that is positive and maximum at zero population and slowly decreases as the population approaches K . Logistic growth is a most natural way to model resource scarcity in a well-mixed system: a population cannot sustain exponential growth indefinitely in a system with limited resources, and its ability to grow will be reduced as resources become scarce. Given the spatial constraints in a cavity and the fact that nutrients are introduced via the mouth of the cavity (and must thus first reach the floor for microbes living there to be able to grow), it is reasonable to introduce it in our study to study its possible effects.

On the other hand, the Allee effect is an effect opposite to logistic growth. It is the effect by which the growth rate of a population increases as the population itself grows (typically at low population densities) [25]. The Allee effect is representative of the phenomenon of cooperation, that by which the presence of nearby individuals enhances one's ability to reproduce or grow. microbes are known to be susceptible to the Allee effect [26–28], and it is thus reasonable to ask what its effect might be on a cavity-like system.

There exists a distinction between a “weak” and a “strong” Allee effect. In a weak Allee effect, the growth rate is always positive, such that the empty/dead state is always unstable (as is the case under regular exponential growth or logistic growth). In a strong Allee effect, on the other hand, the growth rate is initially negative for low population densities and only becomes positive above some population threshold, making the empty state

metastable (if the density is below the threshold, it goes to zero, but will grow if above the threshold). Even though the strong Allee effect might potentially also occur in microbial systems [26, 28], here we shall focus on the simpler case of a weak Allee effect. A population $N(t)$ growing under a weak Allee effect will grow in time according to

$$\partial_t N(t) = b_A(N)N = b(1 + BN)N \quad (2.16)$$

where $b_A(N)$ is the growth rate due to the Allee effect, dependent on the exponential growth rate, b , and the strength of the Allee effect, B .

Considering both effects, the birth term in Equation 2.1 can be replaced by

$$b(\rho) = b\rho(1 - k\rho)(1 + B\rho) \quad (2.17)$$

where k sets the strength of the logistic effect and B of the Allee effect. This general form of the birth function also allows us to study the effects of one type of growth, ignoring the other, by simply setting $k = 0$ or $B = 0$.

Now, we can solve Equation 2.12 with the new birth term to obtain an updated bifurcation diagram. Intuitively, we might expect logistic growth to stabilize the gas phase and push back the onset of jamming, since it reduces the growth rate at higher densities. On the other hand, the Allee effect promotes cell birth and thus is expected to induce jamming earlier than for simple exponential growth. Figure 2.6.A shows the bifurcation diagram when logistic growth is present ($k \neq 0$) in the absence of an Allee effect ($B = 0$). Note how the establishment length is unchanged, since near $\Phi = 0$ the effect of the reduction in the growth rate due to k is negligible. Notice also how, as k grows, the curve for Φ_0 is slowly pulled to the right of the bifurcation diagram, until for some critical value k^* the fold bifurcation from the gaseous to the jammed state disappears and the system presents a transcritical bifurcation, changing continuously from gas to jammed as l is increased, confirming that intuition that logistic growth “gasifies” cavities.

Figure 2.6.B shows the effects of an Allee-type growth ($B \neq 0$) for no logistic growth ($k = 0$). In this situation the establishment length is also unchanged and for the same reason, because near $\Phi = 0$ the effect of the term $+B\Phi$ is negligible. As expected, the curve in the diagram is now pulled to the left as B increases. Now the fold bifurcation does not disappear, but the part of the curve with positive slope, corresponding to the stable gaseous

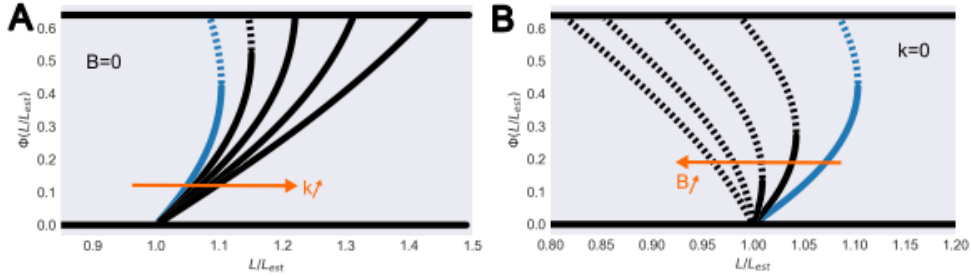


Figure 2.6: Bifurcation diagrams for the packing fraction, Φ_0 , at the floor of the cavity as a function of the reduced length, $l = L/L_{est}$, in the presence of logistic growth or an Allee effect. For reference, the control case without any of the two effects is shown in blue. In all cases, the establishment length remains unchanged. Solid/Dashed curves are stable/unstable steady states, respectively (the horizontal lines corresponding to the empty and jammed states do not show this distinction for ease of plotting). **A)** Effect of logistic growth in absence of an Allee effect. The curve obtained from Equation 2.12 is shifted to the right for stronger logistic growth, and eventually the bistability region and the saddle-node bifurcation disappear and the transition from gaseous to jammed is continuous, allowing also the gaseous state in a larger range of reduced lengths. **B)** Effect of an Allee effect in the absence of logistic growth. The curve obtained from Equation 2.12 is shifted to the left as the Allee effect grows stronger. Eventually, the stable gas phase disappears and the only allowable non-empty stable state is in the jammed phase. Note how the Allee effect permits the presence of populations below the establishment length $l = 1$.

phase, gets smaller. For some critical value, B^* , the gas phase disappears altogether from the bifurcation diagram. This implies that, if the system is in a non-empty steady state, it must correspond to a jammed state. Note also how, when the Allee effect is strong enough, the system allows for stable jammed states even for $l < l_{est}$, as long as these are reached continuously from a jammed state at $l > l_{est}$ thanks to the hysteresis cycle.

It is important to stress this last point, that the Allee effect has the potential to stabilize jammed populations in caves even as the exponential growth rate b of the cells in the cavity falls below the establishment threshold. This can potentially have important ecological consequences. Imagine two

harmful strains of microbes, identical in every way except for the fact that one presents an Allee effect and the other does not. Using an antibiotic that decreases the growth rate of both strains below establishment would potentially be enough to get rid entirely of Allee-free strain, while being practically useless against the strain with the Allee effect.

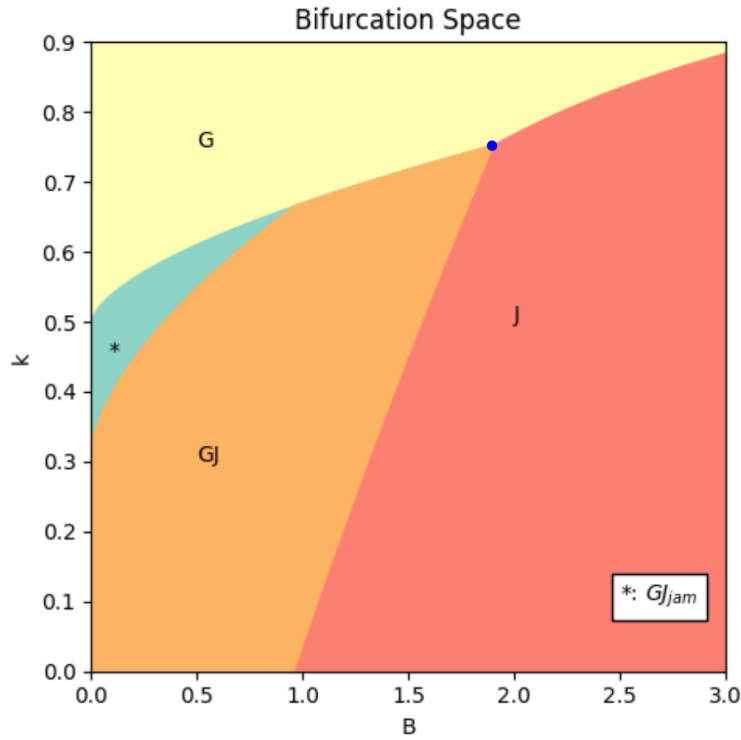


Figure 2.7: Bifurcation space for cavity systems. Each colored region corresponds to a bifurcation diagram showing a distinct set of bifurcations. The orange region (marked “GJ”) corresponds to the existence of the fold bifurcation, as in Figure 2.4. The yellow region (“G”) corresponds to the continuous gas-jam transcritical bifurcation, as in Figure 2.6.A. The red region (“J”) corresponds to the bifurcation diagram where there is no stable gas phase, as in Figure 2.6.B. The green region (“ GJ_{jam} ”) corresponds to the region where the fold bifurcation should exist but the system instead shows a continuous transition due to the presence of the jamming threshold, Φ_{jam} (see main text for details). The blue dot marks the tricritical point.

Figure 2.7 shows the complete bifurcation space of the cavity in the general case $(k, B) \neq (0, 0)$. The bifurcation diagrams presented in Figure 2.6.A and Figure 2.6.B correspond to the x-axis and the y-axis, respectively. The term *phase* here is used to refer to which kind of bifurcation the system presents. It can present the fold bifurcation, such that there are a stable gas phase and jammed phase separated by a discontinuous jump in density at l^* , denoted GJ in the diagram. It can present a stable gas and a stable jammed phase but with a continuous transition between the two as per the effect of logistic growth, denoted G in the diagram. Or, alternatively, it can present no stable gas phase, only the jammed one, as per the result of the Allee effect, denoted J . The fourth region in the diagram, denoted GJ_{jam} refers to the case in which the system would naturally present a fold bifurcation, as in GJ , but instead presents a continuous transcritical bifurcation due to hitting the jam packing fraction, Φ_{jam} . That is, if we were to calculate the curve in the diagram using Equation 2.12 for $\Phi \in [0, 1]$, it would appear to suggest the existence of a fold bifurcation at l^* , corresponding to some Φ^* ; yet, it will not show that because $\Phi^* > \Phi_{jam}$ and thus the system jams without ever reaching Φ^* .

The phase diagram suggests two further things. The first one is the existence of a tricritical point, $(B_{tri}, k_{tri}) = (1.89, 0.753)$ where all of the previously discussed effects come together at once. The resulting phase diagram is surprisingly simple: the curve obtained from Equation 2.12 is simply a vertical line at $l = l_{est} = 1$ implying that, at the establishment transition, any steady state value of Φ up to Φ_{jam} is a possible solution (although the relevance of this in a real system is almost none since any small fluctuation might drive it away from l_{est}). The second one is that, although the experimental setup in [5] is compatible with simple exponential growth, as implied in the paper, it is also compatible with any set of parameters (k, B) in the GJ phase. This means that the microbes in the experimental system might potentially show either the Allee effect or the effects of nutrient depletion without it affecting the overall results of the study, but the effects of non-exponential growth could prove crucial in more critical conditions.

In this section we studied the effects of non-exponential growth on the steady state of the population inside the cavity. Until now, we have kept the condition that the density of cells at the mouth of the cave be equal to zero. In the next section, we shall relax this condition and explore what effects it might have on the steady state of the population.

2.4 Non-zero boundary conditions

So far, we have used the condition that the density of cells at the mouth of the cave is zero (see the discussion around Equation 2.2). We shall now relax this condition and study what happens when there is a constant but non-zero number of cells at the mouth of the cavity.

The first result we shall discuss is that of the *indistinguishability* of density profiles. Suppose we have two density profiles in steady state, $\rho_1(y)$ and $\rho_2(y)$. Suppose that both have the same value at the floor of the chamber, that is, $\rho_1(0) = \rho_2(0) = \rho_0$. Assuming that b and D_0 are the same in both cavities, suppose now that the length of cavity 1 is shorter than that of cavity 2, that is, $L_1 < L_2$. Then, allowing for a non-zero boundary condition at the mouth of the cave, if $\rho_1(L_1) = \rho_2(L_1) = \rho_{L_1}$, the two density profiles are indistinguishable in the interval $y \in [0, L_1]$. This result is obvious if one considers the reaction-diffusion system from Equation 2.1 in the interval $[0, L_1]$ with the boundary condition at L_1 to be $\rho(L_1) = \rho_{L_1}$. Since both system 1 and 2 satisfy the boundary condition and follow the same equation, not only must they have the same ρ_0 at the floor, but also everywhere in $[0, L_1]$. Figure 2.8 shows an example of three indistinguishable density profiles for increasing cavity lengths. This property of indistinguishability has one important consequence: every steady-state density profile, $\rho(y)$ with the boundary condition at the mouth $\rho(L) = \rho_L \neq 0$ can be mapped to a single density profile of length $L' > L$ with the zero-boundary condition at the mouth, simply by extending the curve of $\rho(y)$ from L to L' .

The second consequence of having non-zero boundary conditions at the mouth of the cavity is that the establishment length is always equal to 0. This can be seen from the indistinguishability property, but can more easily be understood in intuitive terms. If one has $\rho(L) = \rho_L \neq 0$ at the mouth, then the mouth of the cavity acts, not as a *drain* of cells, but as a *reservoir*. If the density in the cavity falls below ρ_L , then cells will be supplied from the mouth until the density is, at least, ρ_L everywhere in the cavity. In particular, this implies that the density at the floor of any cavity, in steady state, will satisfy

$$\begin{aligned} \rho(y=0) &= \rho_0 > \rho_L = \rho(L), \quad L > 0 \\ \lim_{L \rightarrow 0} \rho(y=0) &= \rho_L \end{aligned} \tag{2.18}$$

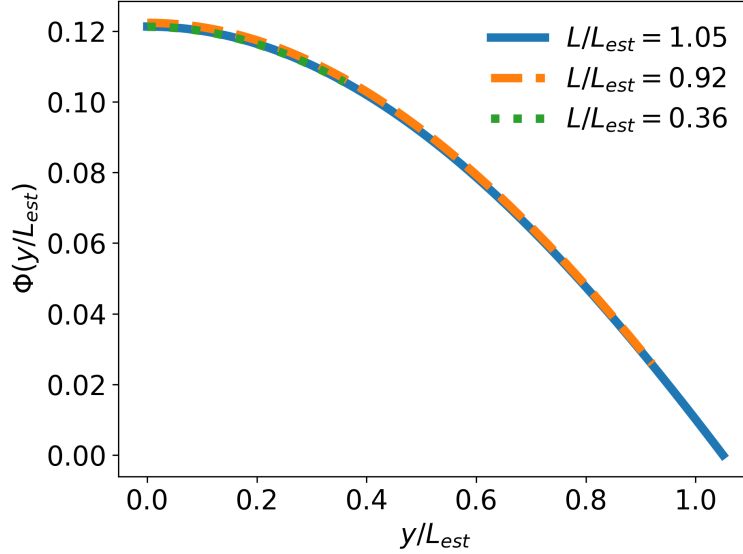


Figure 2.8: Indistinguishability of profiles for $\Phi_L \neq 0$. A profile with some non-0 Φ_L at the mouth of the cavity is equivalent to the profile of some longer cave with a lower value of Φ_L , in particular one with $\Phi_L = 0$. See main text for further discussion.

where L is the length of the cavity.

We can still use Equation 2.12 to predict the value of ρ_0 at the floor of the cavity for a given ρ_L at the mouth for different cave lengths. The resulting curves, plotted for a range of values of ρ_L , are shown in Figure 2.9, in the kind of bifurcation diagrams discussed in Section 2.3. The fact that the establishment is brought to 0 can easily be observed in the diagrams: a cavity that would have been empty in the case of zero density at the mouth will now always be populated with microbes in steady state. In particular, as ρ_L grows, it will even push a cavity into the jammed state that would otherwise be empty (or in a gaseous state) if the density at the mouth were 0. This phenomenon we shall call “Outsider-Induced Population” or “Outsider-Induced Jamming”, since outsider cells coming in from the mouth produce a stable population in the cavity, either in the gas or jammed state. We note also that the density at the mouth needed for jamming to occur need not be disproportionately large.

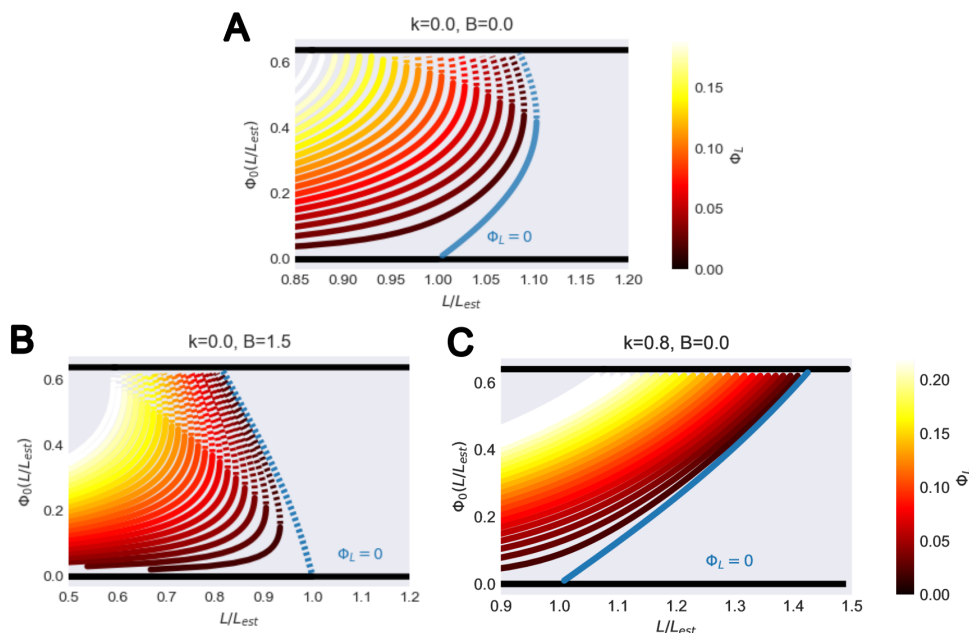


Figure 2.9: Bifurcation diagrams for non-zero packing fractions at the mouth of a cavity. **A)** Diagram in the absence of logistic growth or an Allee effect. **B)** Diagram for a strong Allee effect, in the absence of logistic growth. Colormap is as in C. **C)** Diagram for a strong logistic growth, in the absence of an Allee effect.

Outsider-Induced Population has one deep ecological and evolutionary consequence: Invader-*Sustained* Jamming. Imagine the following situation: there is a cavity, short enough that it would not be able to hold a steady state population of microbes on its own. Imagine now that there is a (more or less constant) density of cells at the mouth of the cave that populates the cavity and causes it to be in the jammed state (for example, the cavity might be a small crypt in the intestine and there might be a significant amount of cells in the intestinal lumen causing this jamming). We shall call this strain A. If, for some reason, cells were to be washed out from the mouth of the cave, then the population inside the cavity would become unstable and it would empty out. Imagine instead that a different strain, B, substitutes strain A at the mouth of, but not inside, the cave (this might occur in the example of the intestine if an invader microbes enters the lumen and drives out the resident strain, populating the lumen by itself), with a similar concentration. This

will keep the remaining cells of strain A inside the cavity in a jammed state. Since the population of A remains jammed, the probability that strain B invades the cavity is practically zero (this is one of the main results from [5], see the Introduction for a deeper discussion). But the fact that B is present at the mouth is *precisely* what is stabilizing strain A inside the cavity! The invader *sustains* the jamming state of the resident strain, which causes the resident strain to become practically immune to invasion.

This Invader-Sustained Jamming has some deep ecological consequences, because it suggests that a strain with a very low fitness for a given environment can potentially survive for long periods by being sustained inside a cavity by other, much fitter, strains while having a low risk of being invaded. If the conditions then change in the system to make the unfit strain become fitter, it could potentially repopulate again the medium outside the cavity and dominate the system. This might have potential consequences in the use of antibiotics, where an invading population that is susceptible to antibiotics might survive inside cavities, only to thrive again the moment the antibiotic is pulled out of the system.

In the following chapters, we will make use of more complex models that will allow us to test and validate the phenomenons of Outsider-Induced Population and Invader-Sustained Jamming.

Chapter 3

Two-Dimensional Models

In the previous chapter, we saw a one-dimensional approach to studying microbial populations in cavity-like environments, which we used to study the different states of the system and the transitions between them, as well as predicting novel phenomena, particularly that of Invader-Sustained Jamming. Perhaps the biggest limitation of the reaction-diffusion approach is that the population of cells is reduced to a single observable, the density, assumed to be continuous in space. While this might be sensible at higher densities, it becomes misleading at very low densities, when stochasticity and the discreteness of the cells cannot be neglected. Moreover, the reaction-diffusion model cannot distinguish any phenomena at the single-cell level. In this chapter we will present more complex models capable of resolving these issues, and we will present them in their two-dimensional version, a more realistic approach to studying the cavities. We will consider three different models: a soft-disk model, a 2D reaction diffusion system and an individual-based model with point-like cells, with a special focus on the latter, since it will serve as the main model used in subsequent chapters. These models will allow us to look at the coexistence of different strains in a cavity (Chapter 4), as well as to study general properties of microbial populations (Chapter 5) and the phenomenon of invasion (Chapter 6).

3.1 Soft-Disk Model

A sensible approach to modeling the microbial population in a cavity is to model each individual cell separately, a so-called individual-based model. In this section, we will briefly cover an approach based on soft proliferating disks, and we will use it to qualitatively test Outsider-Induced Population.

Following [5], we might model the particles as purely repulsive disks, whose interactions upon contact with one another are given by the repulsive potential

$$U_{WCA}(r_{ij}) = \begin{cases} 4\epsilon \left[\left(\frac{\sigma_{ij}}{r_{ij}} \right)^{12} - \left(\frac{\sigma_{ij}}{r_{ij}} \right)^6 \right] + \epsilon & \text{if } r_{ij} < 2^{1/6}\sigma_{ij} \\ 0 & \text{else} \end{cases} \quad (3.1)$$

for any two cells, i and j , where r_{ij} is the interparticle distance, $\sigma_{ij} = (\sigma_i + \sigma_j)/2$, where σ_i is the size of cell i (idem for j), and ϵ is some characteristic energy scale. This potential is known as the Weeks-Chandlers-Andersen (WCA) potential, and simply corresponds to the repulsive part of a Lennard-Jones potential [29]. The corresponding curve for $U_{WCA}(r_{ij})$ is shown in Figure 3.1.

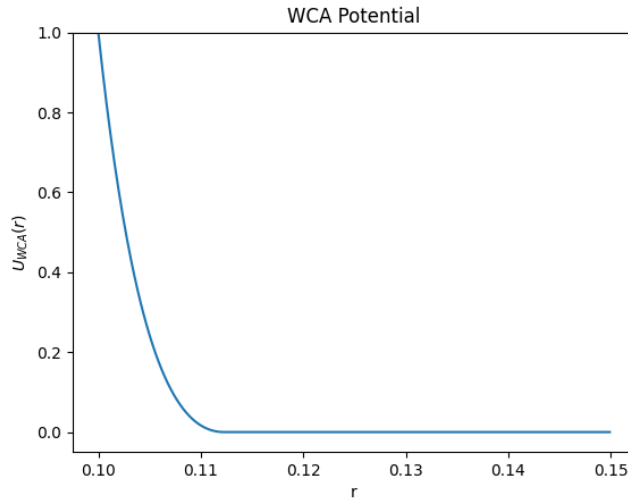


Figure 3.1: WCA Potential with $\epsilon = 1$, $\sigma = 0.1$

On top of the WCA potential, cells give birth to daughters via budding. The mother-daughter pair are kept together via a Hookian spring

$$U_{md} = \frac{\kappa}{2}(r_{ij} - b_{ij})^2 \quad (3.2)$$

where κ is the strength of the spring, and the spring's rest length, b_{ij} , grows with constant growth rate k until $b_{ij} = \sigma_i \equiv \sigma$ (where σ_i is the size of the mother, and a cell is considered mature at size σ), at which point the link between the mother and daughter is severed. The daughter itself also grows in size at rate k , until it reaches maturity at size σ .

Cells in this system move following Brownian motion of variance $2 \cdot D$ (D being the diffusion coefficient), and the interactions with the walls are repulsive of the type

$$U_{wall} = A \cdot e^{-d/\zeta} \quad (3.3)$$

where A is the amplitude of the potential, ζ its characteristic length scale and d the distance beyond the wall reached by the particle, as measured from its center. This confining potential is applied at the floor of the cave and at the side walls, but crucially not at the mouth, where cells are allowed to exit.

The model described above shows an overall behavior that is consistent with the 1D reaction-diffusion system and experiments [5]. It can present an empty cave if the reduced length, l , is small enough (Figure 3.2.A), a gaseous phase for small but higher reduced lengths (Figure 3.2.B), and a jammed phase for large l (Figure 3.2.C), with a discontinuous transition between the two akin to the fold bifurcation described in the previous chapter [5].

This model can be used to test the hypothesis of Outsider-Induced Population and Invader-Sustained Jamming. By introducing cells at the mouth of the cave at different rates, we can mimic the effect of $\rho_L \neq 0$, as described in Section 2.18. In a cave that would naturally be unable to support a stable resident (blue) population (see Figure 3.3.A), introducing invaders (yellow) at a small rate will stabilize a population in the gas state (see Figure 3.3.B), and if the rate of cell input is high enough, the population inside the cavity starts to behave as in the jammed phase (see Figure 3.3.C). Note also how the introduction of invaders seems to push some of the resident cells into the floor of the cavity. This slows down their exit from the cave as, in order to reach the mouth, they must overcome a series of collisions against incoming particles (it must be noted, though, that this effect is exaggerated here by the

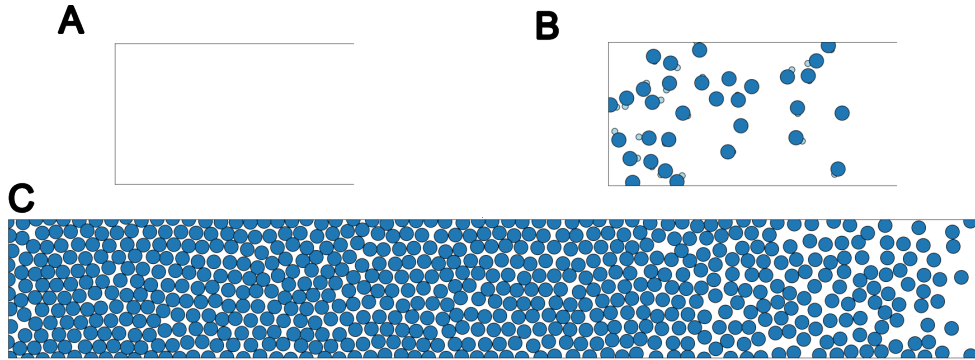


Figure 3.2: Cavities simulated using the soft-disk model in 2 dimensions. **A)** Cavity with reduced length below establishment. Shows an empty steady state. **B)** Cavity in a gaseous steady state. The cells reproducing via budding, and the buds can be appreciated in the image (light blue disks) **C)** Cavity in a jammed state. Notice the tight packing of the disks, how they are in contact with others and how the packing fraction is considerably higher than for a gaseous cavity.

small number of cells and their relatively big size with respect to the cave, a constraint imposed by computational power, or lack thereof, as it constrains the simulations to small systems).

Despite the fact that the soft-disk model is capable of resolving questions at the single-cell level, we would like to construct a model simpler in design, dependent on just a few parameters, that is also useful to extract data at the single-cell level but which also keeps some of the macroscopical properties of the one-dimensional reaction-diffusion model. This will be the object of the next section, and it will serve as the main model in subsequent chapters of this thesis.

3.2 The two-diffusivities model

In this section, we shall describe a novel model that will serve as the main in-silico test-bed for the properties of cave-like systems addressed in the next chapters of this thesis. But before we present the model, we need to discuss the distinction between *self-diffusion* and *collective diffusion*.

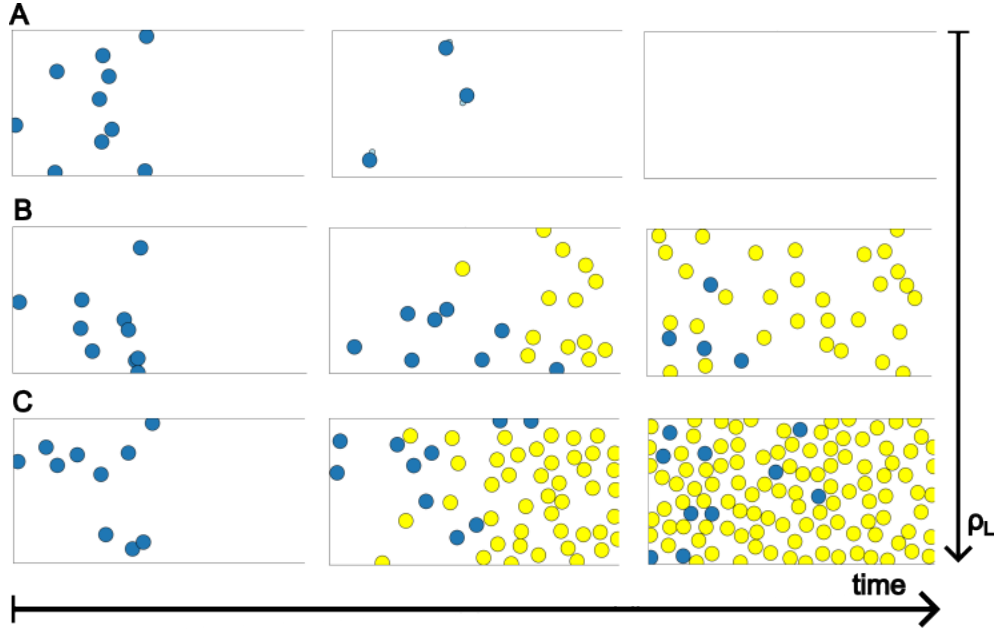


Figure 3.3: Outsider-Induced Population in a soft-disk model of proliferating cells. Three simulations are shown (A,B,C). The initial resident population is marked blue, and the outsider cells are marked yellow. Time increases from left to right, and the density of cells at the mouth of the cave increases from top to bottom. **A)** Zero density of cells at the mouth, $\rho_L = 0$. The cavity cannot support a stable population and is emptied out eventually. Notice also the budding process by which cells reproduce in this model (light blue buds) in the center panel. **B)** Non-zero density at the mouth. Invaders eventually colonize the cavity and stabilize it in a gas phase. **C)** Non-zero density at the mouth, higher than in B. The stabilized population is now in a state similar to the jammed case.

3.2.1 Self-diffusion *vs.* collective diffusion

Consider a single Brownian particle moving according to the overdamped Langevin equation in one dimension:

$$\dot{x} = \sqrt{2D}\zeta(t) \quad (3.4)$$

where x is the position of the particle, D the diffusion coefficient and is constant and $\zeta(t)$ Gaussian white noise. It is well-known that the probability

distribution to find the particle at position x at time t follows the Fokker-Planck equation

$$\begin{aligned}\partial_t P(x, t) &= D \partial_x^2 P(x, t) \\ &= -\partial_x j\end{aligned}\tag{3.5}$$

equivalent to Fick's 2nd Law, where

$$j = -D \partial_x P(x, t)\tag{3.6}$$

is the current of probability. The diffusion coefficient appears both in Equation 3.4 and Equation 3.5, and can be interpreted in two ways. In Equation 3.4, the diffusion coefficient measures the size of the individual “jumps” performed by the Brownian walker at every time step. We shall refer to this diffusion coefficient as the *self-diffusion coefficient* or *self-diffusivity* of a particle. On the other hand, the diffusion coefficient as it appears in Equations 3.5 and 3.6 can be understood macroscopically as the coefficient of proportionality that relates gradients in probability (or concentration/density) to the macroscopic currents generated from those gradients. We shall from now on refer to this “macroscopic” diffusion coefficient as the *collective diffusivity*. Of course, in the simple situation presented here, the self-diffusion coefficient and the collective diffusivity are constant and exactly the same. But this can be generalized to a situation where the self-diffusivity and the collective diffusivity are density-dependent and in general not equal to one another.

In particular, consider the diffusivity function used throughout Chapter 2. This is indeed a *collective* diffusivity, since it relates gradients in density to the currents of cells that they generate. It has the characteristic shape discussed in Figure 2.3, and above the jamming threshold it shoots up by orders of magnitude (ideally to infinity), as any gradient in density is immediately smoothed by the particles pushing on each other.

On the other hand, one can also consider a self-diffusivity that is density-dependent. In general, we might expect that the size of the jumps performed by an individual Brownian particle will decrease as the density of particles around it increases and it has less space available. In particular, when the system hits the jamming density, the self-diffusion of an individual cell will suddenly be reduced by several orders of magnitude and be close to zero: the cell cannot jump around because it is constrained in position by all of the neighboring cells.

This difference in behavior of the self and collective diffusivities is found both in experimental systems of cells in cavities [5] and in soft disk simulations like the ones discussed in the Section 3.1 [5], and it highlights the conceptual differences between the two. It also points out to the need to distinguish them at or near the jamming phase, when the density of cells is very high and the two diffusivities behave in opposite ways, a difference that can be (and is generally) ignored in very dilute systems.

3.2.2 The model

Our aim is to build an individual-based model where the two main independent parameters are the self-diffusivity, D_s , and the collective diffusivity, D_c . We shall model cells as point-like particles that do not interact with each other directly in a pairwise manner as in the soft-disk model. Instead, we want this interaction to occur indirectly via the density, where each cell is pushed/pulled in a given direction by the gradient in the density with a magnitude that is controlled by the collective diffusivity. At the same time, each individual cell will perform a Brownian motion with a jump size mediated by self-diffusivity, in accordance with the expected behavior described in Section 3.2.1. Avoiding the calculation of pairwise interactions greatly simplifies the model, both numerically and analytically. One further restriction we want to impose on our model is that the macroscopic currents come strictly from the collective diffusivity, that is, that self-diffusion should generate no macroscopic currents.

The equation of motion for each individual cell in the system, in this model is

$$\begin{aligned} \dot{\mathbf{x}}_i &= \sqrt{2D_s(\rho)} \cdot \boldsymbol{\zeta}_i(t) + \mathbf{v}_i^{drift}, \quad i = \{1, \dots, N(t)\} \\ \mathbf{v}_i^{drift} &= (D_s(\rho) - D_c(\rho)) \nabla \ln(\rho) + \nabla D_s(\rho) \end{aligned} \quad (3.7)$$

where $N(t)$ is the total number of cells in the system at time t , D_s and D_c are the self and collective diffusivities, respectively, for the cell density $\rho \equiv \rho(\mathbf{x}_i, t)$ measured at the position, \mathbf{x}_i , of the particle at time t , and where all the gradients are with respect to the spatial coordinates. The corresponding drift term, \mathbf{v}_i^{drift} , ensures that any macroscopic current is exclusively driven by D_c . Indeed, the corresponding diffusion equation followed by the total

particle density is

$$\begin{aligned}\partial_t \rho(\mathbf{x}, t) &= \nabla (D_s(\rho) \nabla \rho + (D_c(\rho) - D_s(\rho)) \nabla \rho) + b\rho \\ &= \nabla (D_c(\rho) \nabla \rho) + b\rho\end{aligned}\tag{3.8}$$

where the birth term is added ad-hoc to account for cell proliferation. On top of the movement of cells as per the equations described above, each cell has a birth rate b . For a time step Δt , any cell in the system has a probability $P(\text{birth}) = b\Delta t$ to give birth to a new cell and, at least on average, the rate of change of the density due to births will be given by $+b\rho$. In the model, whenever a cell is born, the daughter is initialized in a random position close to the mother and assigned a tag that identifies it as belonging to the same lineage of the mother. This will become useful when looking at population distributions and strain coexistence. As with the reaction diffusion system discussed in Chapter 2, the population will be stabilized because proliferation of cells will be compensated by outflow at the mouth of the cave.

Note that we shall simulate Equation 3.7 plus stochastic proliferation, and thus we *expect* the density profile measured in the system to follow Equation 3.8, but we do not simulate Equation 3.8 directly.

The particular shape of $D_s(\rho)$ and $D_c(\rho)$ used in the simulations of this model can be seen in Figure 3.4. Once again, though, it must be noted that the exact form of these functions does not affect many of the results, as long as their overall shape and behavior is maintained (in particular, the sharp change in behavior in the jammed phase). Note also that, as discussed in Section 2.2, the packing fraction is the observable ultimately used to determine D_s , D_c and the jamming transition. Therefore, to use density in our simulations, we have given cells a nominal diameter of 1, which brings the jamming transition to $\rho_{jam} = 0.815$ cells/area.

As for the boundary conditions used in this model, elastic collisions with the walls were used. A relevant point needs to be made regarding the numerical treatment of the cell density, $\rho(\mathbf{x}, t)$. The simplest way to implement it is to divide the space of the cavity into a square grid. Ideally, one would have a very fine mesh (let Δx be the side length of one square in the mesh) such that the effect of the density on a cell's movement can be measured at the cell's position with a precision of order Δx . But this carries with it a problem, since bringing Δx close to 0 causes the density to end up binarized: in a really fine mesh, most squares will be empty, and a few will have a

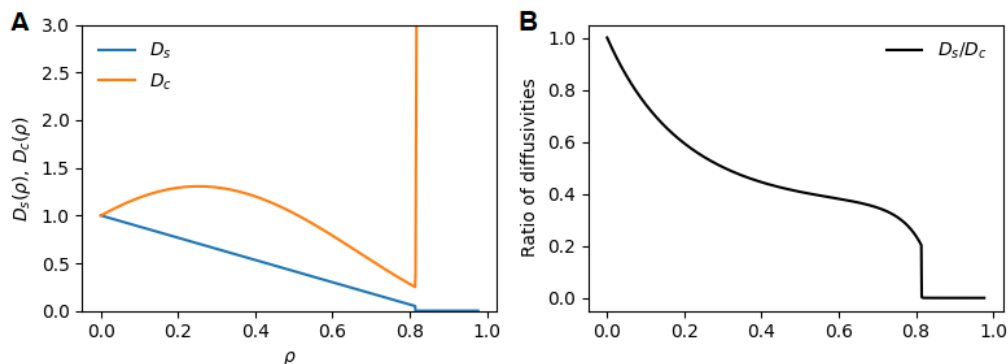


Figure 3.4: **A)** Plot of the self-diffusivity, D_s , and the collective diffusivity, D_c , as a function of cell density. Note that, at the jamming transition $\rho_{jam} = 0.815$, D_c increases by orders of magnitude and D_s drops down to almost zero. **B)** Ratio of diffusivities as a function of cell density. Note how, in the jammed phase, the ratio D_s/D_c drops to nearly 0.

very high value of the density, corresponding to one cell in the very-small space Δx^2 . This problem is solved by using a fine mesh but then smoothing the density profile out using a low-pass filter. Note also that the boundary conditions from Equation 2.2 still need to be satisfied by the density profile.

With all the previous considerations taken into account, Equation 3.7 can be numerically integrated, with the addition of birth processes, for as long as one wishes, yielding the natural evolution in time of an initial population of cells in a cavity.

Figure 3.5 shows two examples of simulations of cavities in 2 dimensions. Figure 3.5.A-C shows a gaseous cavity. The profile shows the characteristic cosine shape, as in the 1D Reaction Diffusion system (green curve in Figure 3.5.B). The cell density at the base is clearly under the jamming threshold and satisfies the no flux boundary conditions at the walls (Figure 3.5.C). Figure 3.5.A shows a snapshot of the actual simulation: each individual dot represents a cell in the system in a similar size to the nominal one used in simulations (needed for the calculation of the packing fraction, from the density). Figure 3.5.D-F, on the other hand, shows a jammed cavity. Note how the density profile is much flatter, and saturated around the jamming density and the density has smaller fluctuations than in the gas cavity (Figure

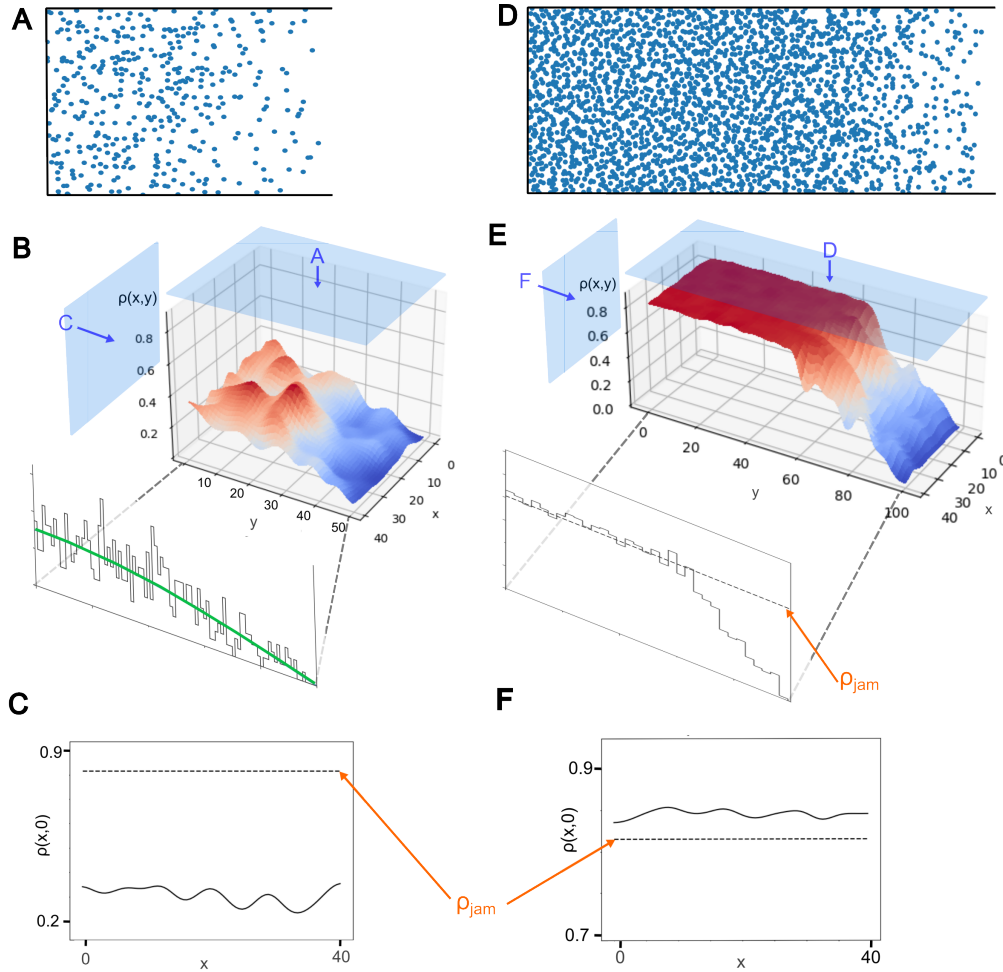


Figure 3.5: Simulations of cavities. **A,D)** Snapshots of a cavity in the gaseous and jammed state, respectively. **B,E)** Density profile in the cavities. The projections show the averaged profile along the length of the cavity. The green curve shows a cosine profile in the gas cavity. The blue rectangles with arrows indicate the projections on which the snapshots and floor-profiles are taken. **C,F)** Density profiles at the floor of the cavities. The jamming density is shown with the orange arrows and drawn as a dashed line. Note how the density at the floor is well below the jamming threshold in the gas cavity and above it in the jammed phase.

3.5.E). In the jammed cavity, the density in the jammed phase is slightly above the jamming density ((Figure 3.5.E-F).

In the next section, we will briefly discuss a reaction diffusion model that is simpler than the model presented here, but can still be used to distinguish cell populations with multiple strains present.

3.3 RD System with mixing

Under some conditions, one might want to study the coexistence of two strains in the system, but with resolution only at the level of density, not the single cell. This is particularly relevant for caves in the jammed phase and to study the coexistence of bands (a phenomenon that will be described in much more detail in Section 4.2), when the density is high and it is sensible to use the continuous approximation. In this section we briefly present a reaction-diffusion model that allows for the inclusion of various strains as well as the distinction between self and collective diffusion. This model is, at the time of writing, being used to study strain coexistence in the jammed phase and, although it yielded no direct results for this thesis, it is useful to understand intuitively the dynamics of strain coexistence in a cavity.

Modifying Equation 3.8, the density $\rho_i(\mathbf{x}, t) \equiv \rho_i$ of strain i in a cavity evolves according to the following equation

$$\partial_t \rho_i = \nabla \cdot \left(D_s(\rho) \nabla \rho_i + \frac{\rho_i}{\rho} (D_c(\rho) - D_s(\rho)) \nabla \rho + b \rho_i \right) + b \rho_i \quad (3.9)$$

where $\rho = \sum_j \rho_j$ is the total density, coming from all strains in the system (including i). Note that if strain i is the only one present in the system ($\rho_i = \rho$), then Equation 3.9 falls back to Equation 3.8, as expected. Similarly, in the case of many strains, the equation for the total density, given by

$$\partial_t \rho = \sum_j \partial_t \rho_j \quad (3.10)$$

also follows Equation 3.8, as expected.

Looking at Equation 3.9, we can gain some more intuitive understanding of the roles of D_s and D_c . The self-diffusion is one which, *by construction*,

will not yield any macroscopic current in the *total* density. But that is not true for a single strain within a multi-strain population. In fact, one can see that the terms in D_s do not cancel out in Equation 3.9. In a system like this, D_s controls the strength of *mixing* currents: even for zero gradient in the total density, if a system has a higher presence of strain i than j in one region and the opposite happens in another region, the gradients in ρ_i and ρ_j will cause them to mix until the system is perfectly well mixed. On the other hand, one can understand the second term, with $(D_c - D_s)$, as producing deterministic collective currents: if D_s gives some current due to randomness and mixing, then the term $(D_c - D_s)$ gives the extra bit of current that comes from *deterministic* forces (i.e. some difference in pressure), dependent on the gradients in total density and felt by all strains proportionally to their relative presence in the system.

These points are exemplified in Figure 3.6, where Equation 3.9 is solved in one dimension for a system composed of two different strains/densities, colored red and blue, in the absence of proliferation, in a system closed on both sides. In Figure 3.6.A, collective diffusion is turned off. Initially, the mix of red and blue is heterogeneous (left panel). As the system evolves, D_s causes the mixing of both densities until, in the end, they are both perfectly mixed (right panel). But, because $D_c = 0$, the total density profile remains unchanged (right panel). On the other hand, in Figure 3.6.B, self-diffusion is turned off. In this situation, and with the same initial profile (see left panel), the total density profile is smoothed out by generating global currents, but in such a way that the two colors will not mix once those global currents disappear (right panel).

There is one important conclusion that we can take from Figure 3.6.B. In a real system where each density represents one strain of microbes, as small as D_s might be, it will never be exactly zero. This will have important consequences in the coexistence of different microbial strains in cavities, as it will make mixing inevitable. We will discuss this in more detail in the following chapter.

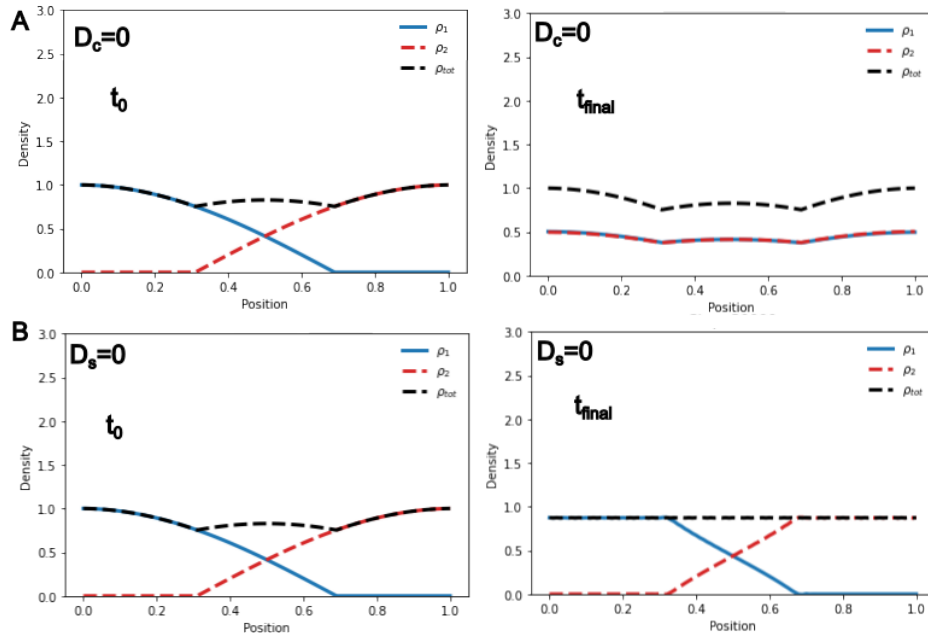


Figure 3.6: Effects of collective and self-diffusion in the creation of currents in a two-density system (painted red and blue; total density colored black). **A)** If collective diffusion is turned off, then self-diffusion only creates mixing currents that do not change the total density profile of the system (no change in the total density profile between the left and right panels). **B)** If self-diffusion is turned off, collective diffusion ensures the total density profile is smoothed out, and once that happens the system remains stable and the different colors do not mix (no mixing of red and blue in the right panel).

Chapter 4

Strain Coexistence in cave-like Environments

In this chapter, we will explore the behavior of caves in both the gaseous and jammed regime using the two-diffusivities, individual-based model presented in Section 3.2. In particular, we will discuss how populations in jammed caves are dominated by the offspring of a few lucky individuals stuck to the floor of the cavity. We will then spend the rest of the chapter discussing strain coexistence in jammed caves. We will focus on the coexistence of *bands* in various regimes: first under neutral competition, then under the effect of selection and lastly under the effect of *pinning*.

4.1 Jammed vs. Gaseous caves

We saw at the end of Section 3.2.2 what caves in the gas and jammed regimes look like, and pointed out to some of the major differences between them in terms of the density profile they present. In this section, we will discuss how those differences affect ecological dynamics inside them.

When a cavity is jammed, cells within the jammed phase undergo a generalized directed motion from the floor to the mouth of the cavity, as a result of the proliferation of cells nearer to the floor of the cavity. Let us see why. If a cell gives birth in the jammed phase, the tight packing means that cells around it have to move in order to make the space required for the child. Since, movement towards the floor and sides of the cavity is limited by the presence of walls, the only way in which the space can be accommodated is by cells moving towards the mouth of the cavity. Since all cells in the cavity keep reproducing, this produces a general flow of cells from the floor to the mouth. This has one very important consequence: virtually any cell in the cavity will be systematically pushed out of the cave by the cells behind it, which leads to the extinction of almost all lineages in the cavity. The only exception to this rule is of course for the cells living at the floor of the cavity. These few lucky cells are in a very privileged position: since they only have the wall behind them, when they reproduce, either they push the child away from the wall and they stay at it or, if they get popped out by the child, then the child itself stays by the wall and inherits the lucky position, meaning the lineage can continue to thrive for a very long time. This phenomenon is observed experimentally [5, 12], and also reproduced in our individual-based model. One consequence of this behavior is that it greatly limits the diversity of a jammed cave, since the diversity outside the floor of the cavity is pushed out, and at the floor the number of cells (and thus the allowed diversity) is very small. Another consequence is that it protects a jammed population from invasion [5]: an invader would have to not only make it into the crowded region of the cavity, but all the way to the floor if it is to have any hope of taking over the entire cavity. The probability of such an event is exponentially small in the length of the jammed phase [5], which protects the resident population from invasion (as we will see in Chapter 6, this holds even when the invader has a huge selection advantage).

Gas cavities, on the other hand, and despite the effects of density dif-

ferences, are not affected by this phenomenon. A cell far from the floor of the cavity can still, through random motion, move away from the mouth, increasing its likelihood of having a higher number of offspring.

In the next section, we will consider one way in which different lineages, or strains, of microbes, can potentially coexist in a jammed cave.

4.2 Bands in a jammed cave

We saw in the previous section how populations in the jammed cave are dominated by a few lucky cells at the floor of the cavity. The question we try to address here is: how can different strains coexist in a jammed cavity?

The answer, as observed in experiments [5, 12] is the formation of *bands*. When two strains of microbes are introduced into a system with many cavities, it will sometimes happen that each of the strains occupies a significant fraction of the floor of a cavity. When this happens, the offspring produced by each of the strains will fill the cavity lengthwise giving rise to bands perpendicular to the floor (see Figure 4.1).

In our individual-based model, generating systems with those kind of bands is extremely simple: one only needs to take a cavity in a jammed state, and assign all cells on one side of a position threshold with one label, and all those on the other side with a different label.

In the next sections, we will address the question of stability of these bands, as well as what happens if we are not in a case of neutral competition and one of the strains has a selective advantage.

4.2.1 Coexistence in the neutral case

Imagine a jammed cavity where two bands have just recently formed from two different strains, occupying half of the cavity each. If the strains are neutral, that is, if both have the same birth rate, ζ will they stably coexist?

The answer is, in general, no. Or at least that is what is predicted by models. To understand why, we must turn to the role of stochasticity and self-diffusion. If we recall the discussion on the reaction-diffusion system in

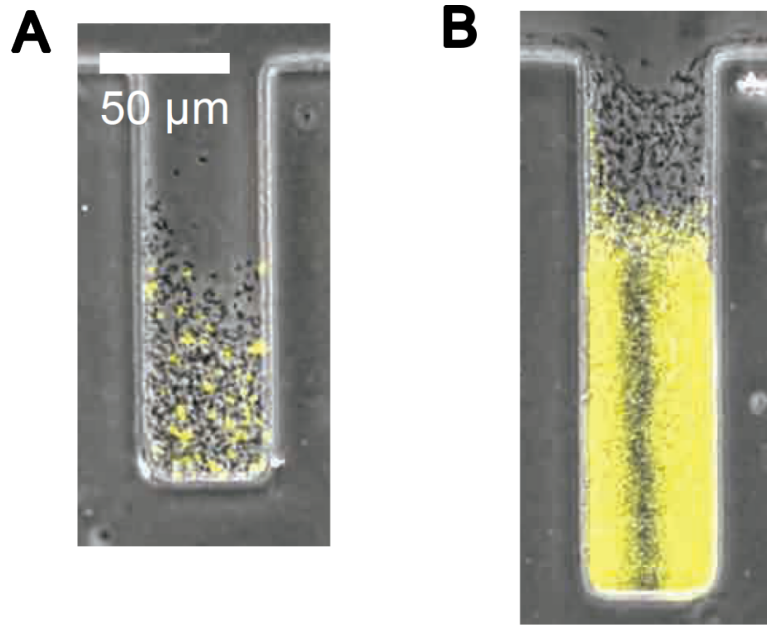


Figure 4.1: *Modified from [5].* Experimental cavities with two strains. **A)** Well-mixed gaseous cavity. **B)** This cavity is in the jammed state and shows the presence of bands.

Section 3.3, as long as $D_s \neq 0$, the densities of different strains in a cavity will eventually mix (think of the density profiles in Figure 3.6 as showing a transversal section of a cave). Since that mixing occurs also at the floor, then the bands are eventually destroyed. If one is not satisfied with the continuous picture, we might turn to the individual-based approach to understand this destruction of bands. Even if one were to completely remove the random drift associated to the presence of self-diffusion, whenever a birth occurs at the floor of the cavity, there is always the possibility that it causes a cell at the boundary between the two bands to be popped out of the floor, thus moving the boundary by about one cell diameter. If there is nothing stopping this drift from happening, then the boundary can be understood as performing some kind of one-dimensional random walk along the floor, which of course leads to the eventual destruction of one of the bands and the fixation of one strain. Figure 4.2 shows a simulation of bands in a jammed cavity under neutral competition, showcasing their natural instability.

Although bands are expected to be unstable, the timescale of their dis-

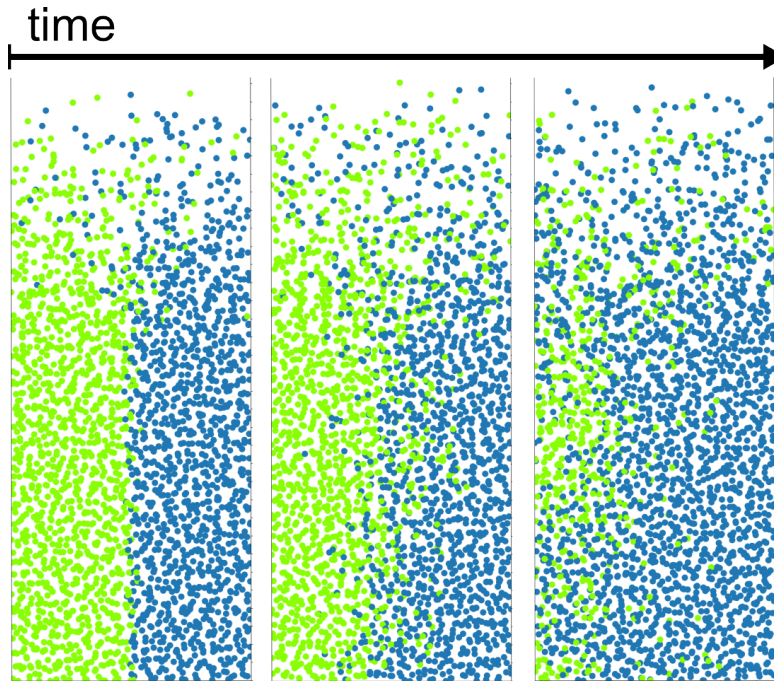


Figure 4.2: Bands in jammed cavities are naturally unstable. Pictured here: a jammed cavity with two bands of strains with the same birth rate. Even in this neutral case, given enough time, the bands mix and whichever strain dominates the floor (in this case blue; see in the center panel how, even if in total the proportion of green vs. blue appears around 50/50, blue is dominating the floor of the cavity.) ends up dominating in the cavity.

appearance is long in the neutral case. In the following sections, we shall explore the effects of selection on band stability and discuss the existence of mechanisms that can stabilize bands.

4.2.2 Selection effects: logistic takeover

Until now, we only considered a neutral situation in which the two coexisting strains have the same birth rate. A natural extension is to consider the case where one strain has a selective advantage over the other. Understanding this setting is particularly relevant for the study of antibiotics, as they might have different effects on the birth rates of strains that are otherwise neutral.

Consider a cavity with two bands of different microbial strains, where one is resistant to antibiotic and the other not. If antibiotic is introduced, one might (correctly) predict that the antibiotic-resistant strain takes over the cavity. But the relevant question is *how* does the takeover process happen? Figure 4.3 shows this takeover in a real experiment where in the initial setup, before antibiotic is added, columns are jammed and forming two bands, one for each strain (Figure 4.3.A, antibiotic-resistant is colored green). After the antibiotic is introduced, there is a rapid process of unjamming of the cavities driven by the reduction in the birth rate of the antibiotic-susceptible microbes (Figure 4.3.B). Meanwhile, the higher relative growth rate of the resistant microbes makes it take over the entire population (Figure 4.3.C). Once it has taken over, and since its growth rate is not much reduced from the antibiotic, it grows rapidly enough to re-jam the cave (Figure 4.3.D, right).

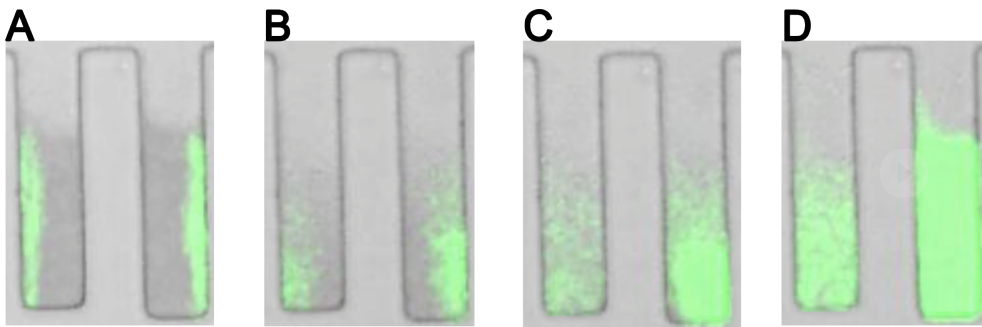


Figure 4.3: Rapid takeover of a cavity by an antibiotic resistant strain, in the presence of antibiotic, destroying the bands present. **A)** Initial state. Both cavities present two bands. **B)** Initial unjamming of the cavities due to the introduction of antibiotic. **C)** At some point, green has taken over most of the cavity, which is still in the unjammed/gaseous state. **D)** As the resistant microbes proliferate, they re-jam the cavity (visible on the right cavity).

Note in Figure 4.3.C, how the left column seems to have unjammed completely, whereas the right column still appears to show some jamming near the floor of the cavity (noticeable by the brighter and more homogeneous fluorescent color). This leads to the first important question: *for a cave initially showing bands, where one strain is antibiotic-resistant and the other is not, is there a way to determine when there is complete or partial unjamming in a cave when antibiotic is introduced? And, is there the possibility that a cavity will remain jammed even in the presence of antibiotic?*

Whether a cavity unjams or not during the process of takeover can have significant ecological consequences. Imagine a situation where the microbes susceptible to antibiotic are pathogenic and one wishes to remove them from the system, while the resident strain is resistant to the specific antibiotic used. If the antibiotic is pulled out of the system before the pathogens have been driven out completely, whether a cavity gasified or remained jammed might have opposite consequences. If it gasified, then the resident strain will most likely repopulate the entire floor of the cavity, pushing the pathogen out as it reams the system. If the cavity did not fully unjam, on the other hand, then whatever bands remain at the floor will simply regrow and, even in the case of neutral competition, the pathogen might end up taking over the entire cave thanks to drift. Understanding when a cavity unjams and when it does not in the presence of antibiotic is thus a relevant question to consider.

Although there is no formal argument to justify this result yet, one finds that the average birth rate of all cells in the system *right after the introduction of antibiotic*,

$$\langle b \rangle = \frac{1}{N} \sum_{n=1}^N b_n \quad (4.1)$$

where N is the total number of cells in the system and b_n is the birth rate of any given cell, is a good empirical indicator of what will be the effect of antibiotics on the unjamming of the cavity. The effects can be summarized as follows:

$$\langle b \rangle = \begin{cases} \ll b_{est} \Rightarrow \text{Full unjamming} \\ \lesssim b_{est} \Rightarrow \text{Partial unjamming} \\ > b^* \Rightarrow \text{No unjamming} \end{cases} \quad (4.2)$$

where, for a fixed cavity length, and following our usual notation, b_{est} and b^* are the birth rates at establishment and jamming, respectively.

Let's try to understand Equation 4.2. A given $\langle b \rangle$ points to a certain steady state as per the discussions in Chapter 2. But, since $\langle b \rangle$ itself depends on time, the dynamics become slightly more involved. In a system with a fraction $x_G(t) = N_G/N$ of antibiotic-resistant cells at time t (denoted G for "Green" in reference to their color in figures), the average growth rate is

$$\begin{aligned} \langle b \rangle(x_G(t)) &= b_G x_G(t) + b_B (1 - x_G(t)) \\ &= b_B + b_r x_G(t), \quad b_r = b_G - b_B \end{aligned} \quad (4.3)$$

where b_G is the growth rate of antibiotic-resistant cells and b_B is the growth rate of the strain susceptible to antibiotic (denoted B for “Blue/Black”, as in the figures) and b_r is the difference in growth rate between both strains. The fraction of antibiotic-resistant cells, $x_G(t)$, is expected to be a monotonically increasing function of time after the antibiotic is introduced (at least on average), and therefore so is $\langle b(x_G(t)) \rangle$. If, upon introduction of antibiotic in the cavity, the average growth rate is larger than b^* , it will remain so for the duration of the experiment, implying that the cavity will stay jammed throughout (third case in Equation 4.2). If, right after the introduction of antibiotic, the average growth rate is much smaller than the establishment threshold, the cavity will fully unjam because the unjamming process happens in a much smaller time frame than the time it takes for $\langle b \rangle$ to recover to a value above b^* (first case in Equation 4.2). Only when the growth rate falls slightly below b_{est} will one have partial unjamming: the system initially tends to unjam, but the average growth rate grows beyond b^* in a short enough time, re-jamming the cavity before it has time to fully unjam. The individual-based model is capable of reproducing all three situations discussed above. Figure 4.4 shows three simulations showing no unjamming (Figure 4.4.A), partial (Figure 4.4.B) and total unjamming (Figure 4.4.C) upon antibiotic introduction, each with the corresponding value of $\langle b \rangle$ immediately after antibiotic introduction.

The dependence of $\langle b \rangle$ on $x_G(t)$ raises a question on the possibility to quantify how the antibiotic-resistant strain takes over a cavity, that is, understanding the dynamics of $x_G(t)$. The resulting form, given in the following statement, is likely to be the most significant quantitative result of this thesis:

In a jammed cavity containing bands belonging to two different strains of microbes, one of which is resistant to antibiotic and the other not, and if there is no physical element preventing the boundary that separates the bands from moving, then the fraction of resistant microbes in the cave, x_G , will grow in time upon the introduction of antibiotic according to the following logistic differential equation:

$$\frac{\partial x_G(t)}{\partial t} = b_r x_G(t)(1 - x_G(t)), \quad b_r = b_G - b_B \quad (4.4)$$

where b_r is the difference in growth rate between that of the resistant strain,

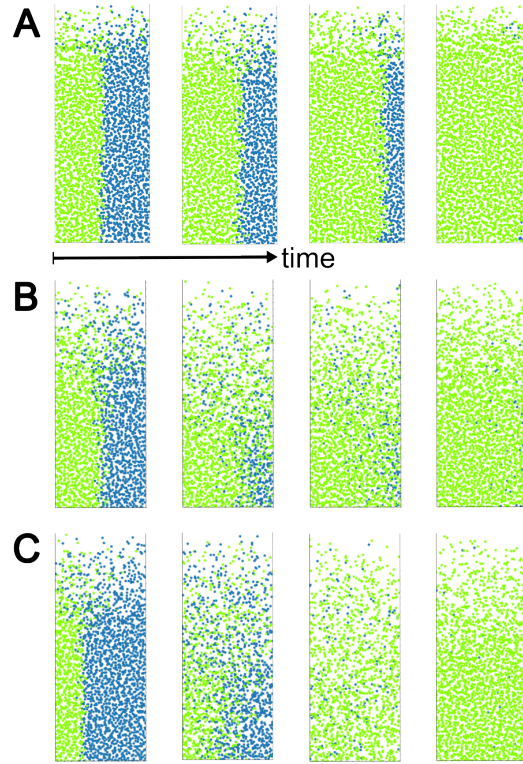


Figure 4.4: Unjamming dynamics of cavities upon introduction of antibiotic. **A)** No unjamming. The resistant strain takes over the cavity and the inter-band boundary remains mostly parallel to the length of the cavity. **B)** Partial unjamming. The cavity unjams but not totally, and the takeover near the floor happens at the edge between the jammed and gas phases. **C)** Full unjamming. The cavity first unjams, then takeover happens in the gas phase, and finally cell proliferation re-jams the cavity.

b_G , and the susceptible strain, b_B . The solution of the previous equation is

$$x_G(t) = \frac{1}{1 + \frac{1-x_0}{x_0} e^{-b_r(t-t_0)}} \quad (4.5)$$

for an initial fraction $x_G(t_0) = x_0$.

This kind of growth will occur, regardless of the state of the cavity with regards to jamming, after the antibiotic is introduced.

There are two interesting observations regarding Equation 4.4. The first is

that this is the same result as one would expect from a *well-mixed* population in which one strain has a significant selection advantage, even though a cavity has a clear spatial structure and the population inside is far from being well-mixed. The second is that this logistic growth occurs *regardless* of whether the cavity unjams or not after the antibiotic introduction, once again pointing to the irrelevance of the spatial structure of the bands.

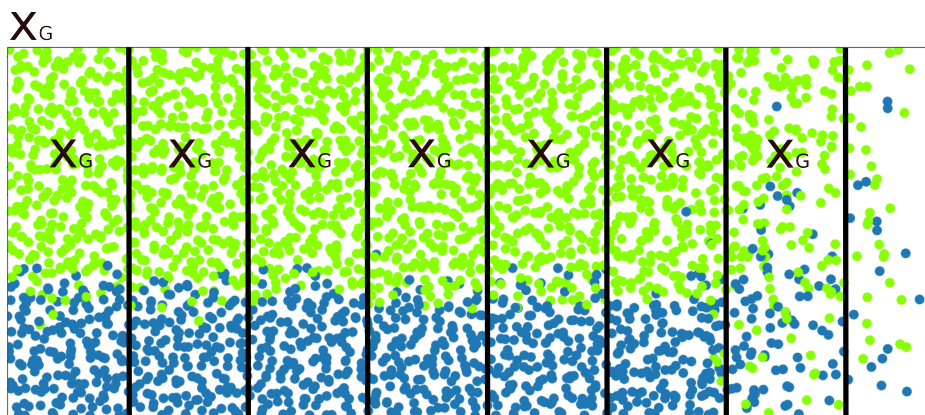


Figure 4.5: Heuristic argument for the logistic takeover of the cave by the resistant strain. If the fraction of resistant cells, x_G , in any section of the cavity is, on average, the same and equal to the total fraction of resistant cells in the cavity, then the outflux of cells at the mouth does not change x_G and the change must come from the difference in birth rates, yielding logistic takeover.

There is a simple way to justify the form of Equation 4.4, illustrated in Figure 4.5. Imagine a cavity with two bands where the resistant strain takes up a total fraction x_G in the number of cells. If the boundary that separates the bands is parallel to the length of the cavity, then any transversal section of cave also contains a fraction x_G of resistant cells. Closer to the mouth of the cavity, where the population is in a gas state, one might expect to find a situation that is approximately well-mixed, and therefore there should also be a fraction x_G of green cells. This means that the proportion of resistant cells that exits the cave through the mouth is, at least on average, also expected to be x_G . This implies that the outflow of cells does not affect the fraction x_G of resistant cells inside the cavity. The only way in which x_G can change in time is thus due to birth rate differences, and the curve for logistic growth duly follows. Figure 4.6 shows the curves for $x_G(t)$ in the same three simulations,

with no unjamming (Figure 4.6.A), partial unjamming (Figure 4.6.B) and total unjamming (Figure 4.6.C), shown in Figure 4.4. The prediction of logistic growth matches exactly the empirical behavior. Comparisons with experimental data will be done in Section 4.4.

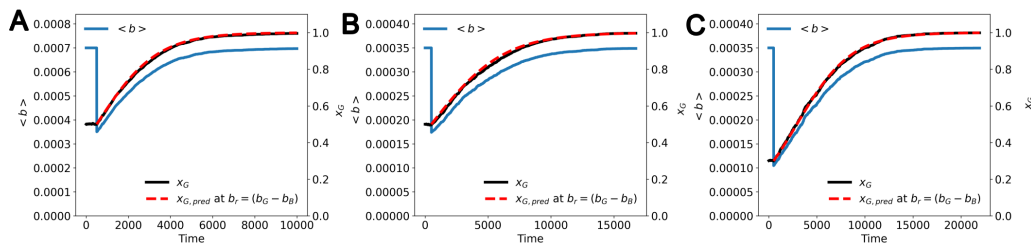


Figure 4.6: Growth curves for the fraction of resistant cells, x_G , and the average birth rate, $\langle b \rangle$, in cavities, upon the introduction of antibiotic. The curves correspond to the same simulations shown in Figure 4.4. **A)** Cavity where no unjamming occurs. **B)** Cavity with partial unjamming. **C)** Cavity with complete unjamming.

The fact that takeover by the antibiotic resistant strain is logistic is also useful because it has a predictable timescale, implying that one can estimate, a priori, how long antibiotic must be present in a cavity for the resistant strain to take over.

The natural question that follows from the expectation of logistic growth is to ask if there is any situation in which it fails and, if so, which one and how does it affect the takeover process by the resistant strain. In the following section we will explore one such instance.

4.3 Stabilization of bands by pinning

Even if the prediction of logistic takeover by the antibiotic-resistant strain in a cavity holds in some experimental situations, it is to be expected that it will break down at some point. One such situation (not treated in this thesis) is if the birth rate difference between the two strains is not sufficiently large for the deterministic approximation to hold, in which case stochastic effects will play a relevant role and the disappearance of bands will be akin to the one described in the neutral case in Section 4.2.1. Another is if there

is some external factor preventing the takeover process from occurring as the theory predicts.

Despite the general instability of bands observed in experimental setups, there are cases in which bands remain stable for a significant amount of time [5], even in the presence of antibiotic and for significant growth rate differences. ¿What drives such stability?

We have seen so far that the formation of bands is dominated by a few cells at the floor of a cavity, and that their instability is (selection effects aside) mainly due to the effects of stochasticity at the floor (see Section 4.2.1). The natural assumption is thus that a band-stabilizing mechanism must act at the floor of the cavity. One such possibility is that the microbes in the cavity develop a biofilm and stick to the walls either naturally or because of the presence of antibiotic, a phenomenon that is well-known to occur when microbes are put under stress [30, 31]. A different possibility altogether is that impurities at the floor of the cavity form a physical barrier that cells would have to cross in order for a band to take over.

In this section, we shall investigate this impurity-driven pinning of bands in a cavity using the individual-based simulations. Possibly the simplest pinning mechanism is a one-dimensional wall (or “pin”) of length L_w , sticking out from the floor of the cavity at the boundary separating the two strains, where the usual no-flux boundary conditions are applied (i.e.: cells are explicitly forbidden from crossing the pin).

Figure 4.7 shows the results from a simulation with two strains, with one that is antibiotic-resistant, in which the length of the pin, L_w , is equal to one cell diameter. Such a small pin is enough to stabilize bands temporarily, even if one of the strains has a significant selective advantage. The corresponding curve for the growth in time of the fraction of antibiotic-resistant cells, $x_G(t)$ is plotted in Figure 4.7.C. Notice how the fraction of resistant cells initially grows in time following the expected logistic curve until it suddenly stops, very abruptly, corresponding to the pinning of the growing band into a stable shape. One might be surprised that the antibiotic resistant fraction of the population grows according to the logistic equation in the beginning, despite being prevented from flowing across the pinning impurity at the floor. This suggests that small deviations from the straight boundary assumption do not greatly affect the prediction of logistic growth. Notice also how, eventually, the resistant cells at the floor of the cavity overcome the pinning boundary,

overflowing it and getting back into the takeover phase, once again following the logistic growth curve. If instead, one places a longer pinning impurity, then the expectation might be that that is enough to prevent overflow by the resistant strain and the complete takeover of the cave. This is shown in Figure 4.7.B, for an impurity with length L_w five times a cell diameter, along with the growth curve for the fraction of resistant strain (Figure 4.7.D). In this case, the boundary reaches some stable shape and remains there, and any attempts by the resistant strain to overflow it are pushed back by the antibiotic-susceptible cells growing from the floor of the cavity.

There is, in fact, an analytical prediction for the expected shape of the boundary separating the two strains in the presence of pinning (see Appendix A.2, full credit goes to Dr. Valentin Slepukhin for this analytical result), given by:

$$\log(y) = \frac{b_{low}}{b_r} \log\left(\frac{x}{1-x}\right) + C \quad (4.6)$$

where $y(x)$ is the corresponding boundary curve (y is the position along the length of the cavity, x along the width and $x \in [0, 1]$ is normalized with respect to the cavity width), $b_{low} = b_B$ is the growth rate of the antibiotic susceptible strain, $b_r = b_G - b_B$ is their difference in growth rates, and C is a constant dependent on boundary conditions. Figure 4.8 shows a simulation with bands pinned by the same impurity as in Figure 4.7.B, along with the prediction for the curve of the boundary between the bands, shown in red.

One interesting question that arises from this pinning analysis, which will not be covered in this thesis, is the study of how the resistant cells might overcome the pinning barrier. The process is likely to be dominated by stochasticity, and a sensible first approach would be to consider the pin as a potential barrier that a given cell might overcome through fluctuations: the longer the pin, the larger the potential barrier and the less likely that a cell will jump across it at any one given time. If one could accurately describe this phenomenon, one might be able to give a complete description of the band takeover of cavities, one that includes both the deterministic part associated to the logistic curve and the stochastic part associated to the barrier-overcoming process.

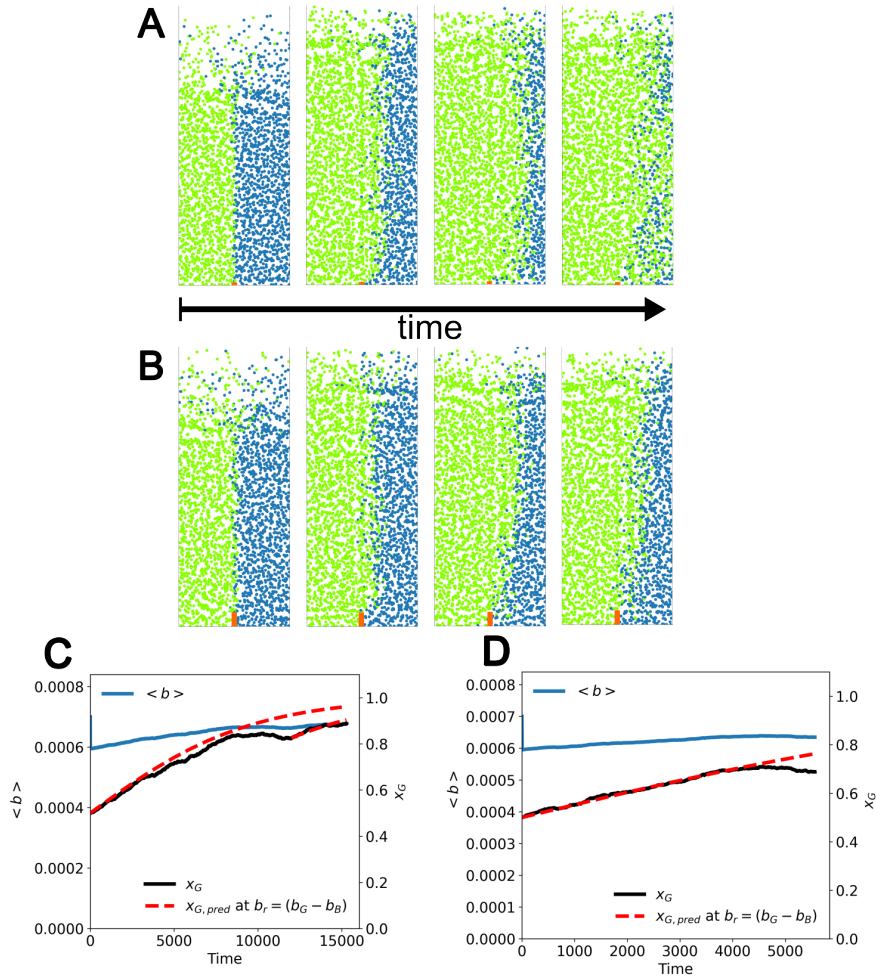


Figure 4.7: Simulations of cavities with pinning at the floor (shown as orange rectangles in A and B, the width is exaggerated to enhance visibility), which difficults the takeover by the resistant strain. **A)** Pinning boundary of one cell diameter. The resistant strain initially starts to take over. At some point it stops due to the pin. Eventually, it overflows the pin and continues to take over. **B)** Pinning boundary of five cell diameters. The pin is large enough to prevent complete takeover by the resistant strain. **C)** Empirical growth curves for the average birth rate (blue) and the fraction of resistant cells (black), and logistic predictions (dashed red lines), for the simulation in A. **D)** Similar to C, for the simulation in B.

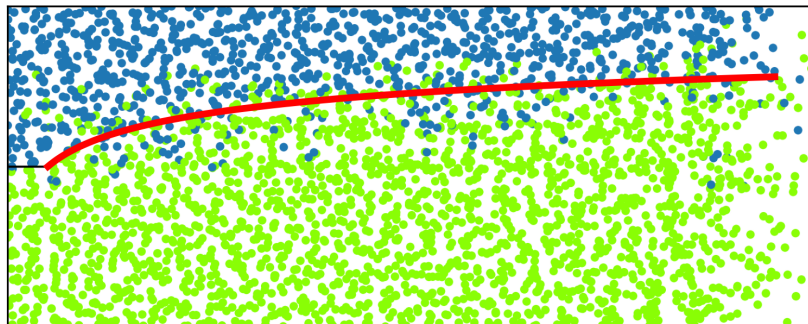


Figure 4.8: Simulation of a takeover process with a pin of length equal to five cell diameters, as in Figure 4.7.B. The red solid line is the prediction of the stable inter-strain boundary under pinning, from Equation 4.6.

4.4 Comparison with experiments

So far, all of the ideas discussed in Sections 4.2.2 and 4.3 stemmed from the dynamics of the individual-based model and were only applied and tested on it. The natural extension is to study how well these predictions apply to real experimental data, if they apply at all.

Fortunately, we received a set of experimental recordings of cavity systems, in the shape of panflutes, made by Dr. Yuya Karita, showing this phenomenon of cavity takeover by one of two strains after the introduction of antibiotic. Two snapshots of the experimental setup can be seen in Figure 4.9.A, at the initial and final frames of the recording. The panflute systems displayed here show a very diverse cavity behavior. In particular, we analyzed six caves (labeled in white in Figure 4.9.B; the antibiotic resistant strain is fluorescent and shown in white color), to test the hypotheses presented in the previous sections.

To carry out the analysis, we used the Software ImageJ [32]. We used the images in black and white from Figure 4.9.B. We considered the average brightness of a jammed, white cavity (i.e.: completely taken over by the antibiotic-resistant strain), I_{max} , to correspond with a fraction of resistant/fluorescent cells $x_f = 1$, and estimated the value of $x_f(t)$ at other times

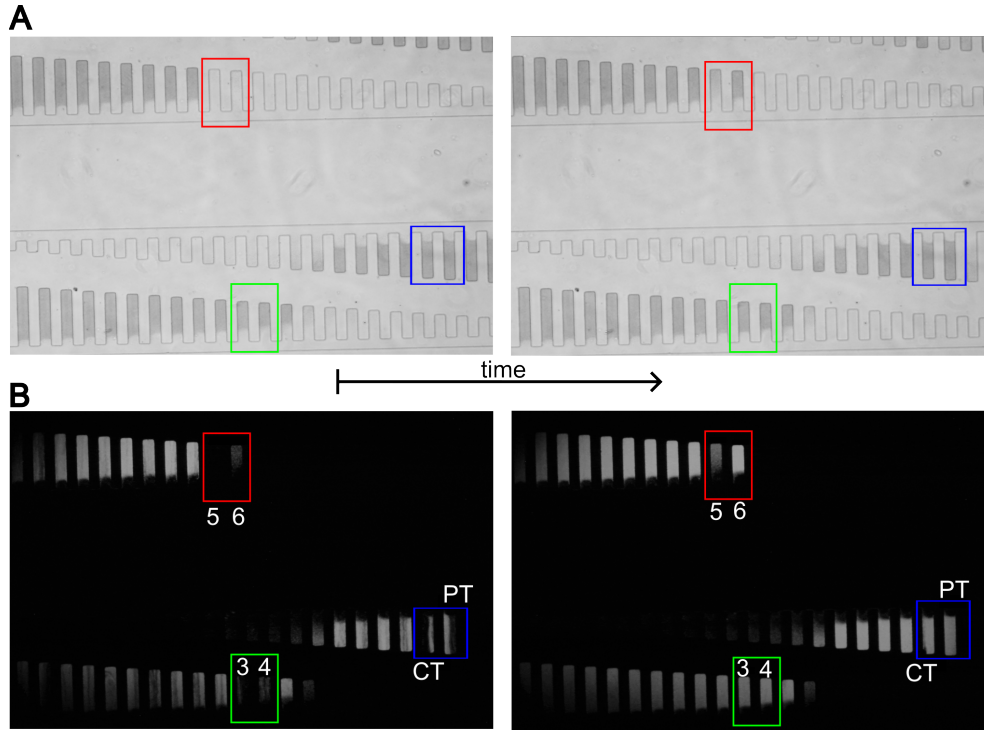


Figure 4.9: Experimental system with three panflutes containing caves of different lengths, shown at the initial (left) and final (right) time of recording. The cavities used in the analysis are shown inside the colored squares. **A)** System as seen through an optical microscope. **B)** Same images as in A, but with the antibiotic resistant strain enhanced in white (the rest, including the other strain, is colored black). The cavities used for the analysis are labeled in white.

from the relative intensity of the white-colored region:

$$x_f(t) = \frac{I(t)}{I_{max}} \quad (4.7)$$

where the intensity, $I(t)$, is taken to be the averaged RGB value of all pixels in the cavity, in the usual RGB scale from 0 to 255. This analysis relies on the assumption of a linear relation between the number of resistant cells in the cavity and the intensity measured in RGB. Linearity will of course break at some point, in particular for high values of I , when the light intensity is expected to saturate. Regardless, in the images from Figure 4.9 the maximum

measured intensity is (in RGB) $I_{max} \sim 100$, less than a third of the maximum allowed value of 255, making the linear assumption plausible.

Figure 4.10 shows the results of the analysis for all caves labeled in Figure 4.9.B. We shall start discussing the analysis of the cavity labeled “PT”, corresponding to “Parallel Takeover” by the resistant strain, where “Parallel” implies that the inter-band boundary remains straight and parallel to the sidewalls of the cavity throughout the experiment (Figure 4.10.A). Takeover in this cavity occurs completely in the jammed phase and the corresponding curve for $x_f(t)$ is consistent with the logistic growth curve of Equation 4.5. Figure 4.10.B shows a cavity where the boundary that separates the resistant and susceptible strains appears to be curved (“CT” for curved takeover). The discussion on pinning made in Section 4.3 makes this a prime candidate to test for pinning at the floor, which we shall explore in the next section. Indeed, the experimental growth curve appears to follow a similar pattern to that observed in pinned boundaries in simulations (see Figure 4.7), where it initially follows logistic growth but at some point suddenly plateaus. Figures 4.10.C, 4.10.D and 4.10.F all show cavities in which takeover happens initially in the gas phase, followed by eventual jamming. The curves of all three cavities appear to show a significant deviation from logistic growth, where the resistant strain appears to take over faster than the prediction. The reason this happens is precisely because of the jamming wave, and we will discuss this in more detail later in this section. Finally, the cavity shown in Figure 4.10.E shows takeover fully in the gas phase: the initial fraction of resistant cells is almost zero, and by the time the experiment is ended it is not yet high enough to cause jamming in the cavity. Still, the agreement with logistic growth is very good, consistent with a large growth rate difference between the two strains in the cavity.

One remark about all the cavities in Figure 4.10 is that, early on in the experiment, they all appear to grow slower than the logistic prediction. Although experimental recordings were started 2 hours after antibiotic introduction to allow for thermal equilibration, it is very likely that the effects of antibiotic set in gradually and that it takes longer than the equilibration time for it to have the full effect. To compensate for this, all fits in Figure 4.10 were done from 3h45min after the initial time of recording.

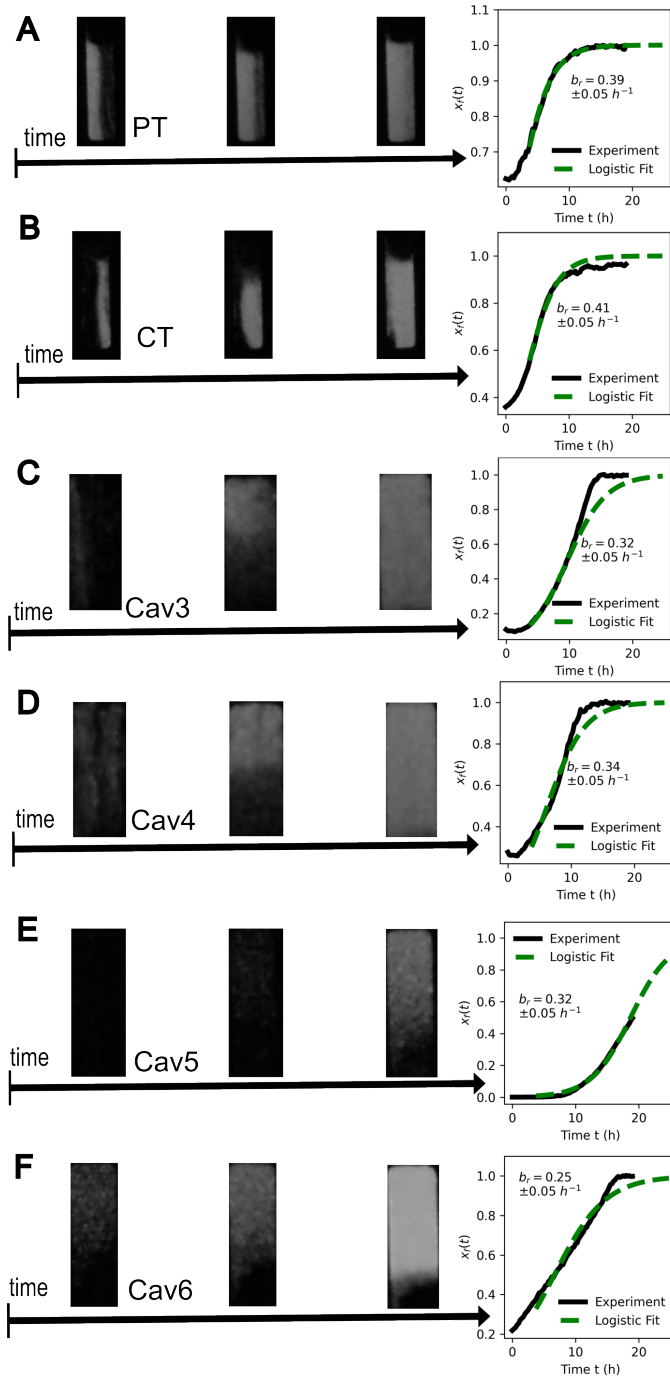


Figure 4.10: Examples of logistic takeover. Cavity snapshots at different times are shown on the left, and the growth curves for the fraction, $x_f(t)$, of antibiotic-resistant cells inside the cavity on the right (black: experimental; green: logistic fit); errors in the growth rates are estimates. Cavity labels are the same as in Figure 4.9.B. **A)** Parallel takeover, without pinning. **B)** Curved takeover, with pinning. **C-D,F)** Takeover in the gas phase. Columns show increase in takeover rate with respect to logistic growth due to a jamming shockwave. **E)** Takeover fully in the gas phase. Does not reach jamming in experimental time.

4.4.1 Pinning in experimental cavities

As discussed earlier, the curved shape of the inter-band boundary in Figure 4.10.B and the deviation of the growth curve from the logistic expectation suggest that there might be pinning affecting the movement of cells at the floor of the cavity.

To test such a possibility, we tracked the wavefront of the inter-band boundary for the cavity with curved takeover at two different points in the cavity: near the floor of the cavity, where we can check if there is pinning; and halfway through the cavity, which we can use as a control (see Figure 4.11.A) since we don't expect pinning to occur there. We also applied the same analysis to the "PT" cavity, where pinning would not be expected at all, as a further control (see Figure 4.11.B). The tracking of the moving wavefront was achieved by binarizing the intensity readings in the recorded cavities and tracking the point of transition in color from black to white. The resulting curves seem to indicate that there is some pinning in the case of the curved boundary, as its movement near the floor of the cavity stops completely at around $t \approx 7.5h$, which does not happen at the midwave. It only seems to start moving again at the floor around $t \approx 16h$ (a fact that is backed up by video recordings of the cavity). This final movement might correspond to the overflow of the cells over the pinning barrier at the floor of the cavity, as discussed in Section 4.3. Also, the pinning of the floor occurs 1 to 2 h before the logistic growth curve in Figure 4.10.B starts to plateau. Although a reliable quantitative analysis is difficult, the observation is qualitatively consistent with the analysis from the individual-based model in Section 4.3, in which takeover is expected to be logistic even in the presence of pinning until the stable curve of the boundary is reached, at which point growth it is expected to stop.

4.4.2 Jamming wave

The cavities in Figure 4.10.C, D and F show a significant deviation from the expected logistic growth curve, with a growth rate that is faster than the prediction. One hypothesis is that this increase in growth rate is caused by the transition from a gaseous to a jammed population in the cavity during the takeover process, which we shall now discuss.

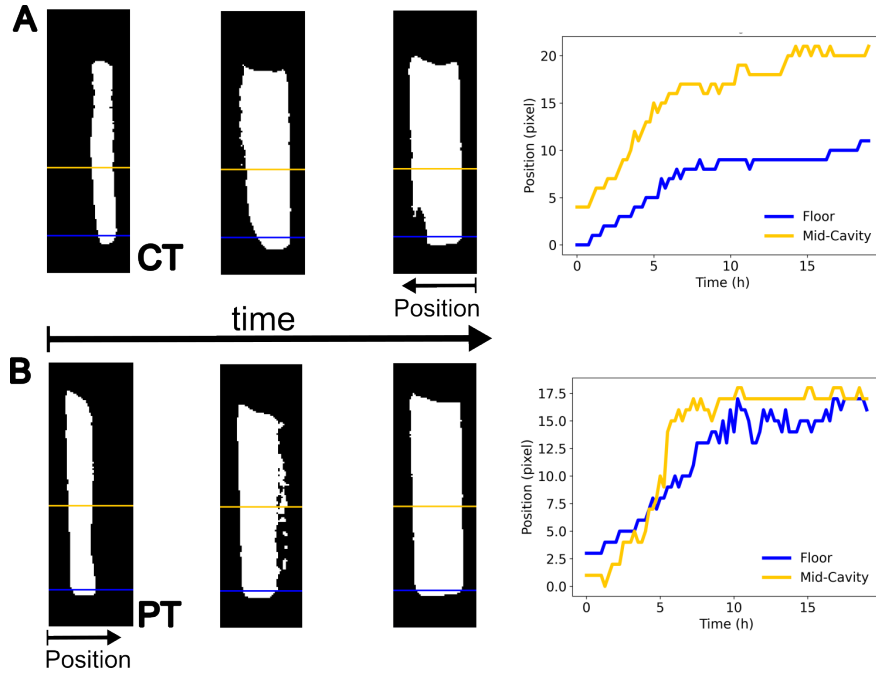


Figure 4.11: Analysis of pinning behavior for the “CT” and “PT” cavities, as labeled in Figure 4.9. **A)** Analysis of the cavity “CT”, whose curvature of the inter-band boundary is indicative of the presence of pinning. *Left:* snapshots of the takeover process by the resistant strain. The analyzed positions along the middle and the floor of the cavity are colored orange and blue, respectively. *Right:* Position (in pixels with respect to the rightmost recorded position) of the inter-band-boundary with time, at the two colored positions. Notice how the wave along the floor (blue) stops moving at $t \approx 7.5$ h, even as the boundary keeps moving at its center (orange). **B)** Same setup as in A, for the “PT” cave, which presents an inter-band boundary that is always parallel to the length of the cave, indicating that there is no pinning present. *Left:* Same as in A. *Right:* Same as in A. In this instance, there is no pinning of the boundary at the floor of the cavity: the wave at the floor never stops moving, and slow-down only happens as it reaches the rightmost wall, as with the marker at the midwave.

We already saw in Section 4.2.2 that, when the presence of antibiotic-resistant cells at the floor of the cavity is large enough, they will cause the population inside the cave to jam. When the jamming occurs, the growth

from the cells in the jammed phase from the floor of the cavity will physically push out of the cavity the cells nearer to the mouth. If the jamming transition occurs when there are still antibiotic-susceptible cells in the cavity, then their disappearance from the cavity will be driven by this jamming wave instead of the selection process. Since the the jamming wave phenomenon occurs much faster than the takeover due to selection effects, this translates into a growth curve with a much steeper slope.

To test this hypothesis, one can compare the growth of the resistant strain in the entire cavity with that near the floor. Close to the floor, the effects of the jamming wave are minimized, and therefore one would expect that there the takeover happens as per the logistic prediction. The result of such analysis on cave “Cav3” is shown in Figure 4.12. After correcting for the effect of this jamming wave, the takeover process agrees with the expectation of logistic growth. Similar results are found for the other two cavities affected by this phenomenon (figures not shown).

It would be reasonable to wonder why this jamming wave was not predicted in the individual-based model. The reason is simply that, in the one simulation in the model that shows complete unjamming, the re-jamming of the cave occurs once the antibiotic-resistant strain has taken over the entire cavity, at which point there are no susceptible cells left that can be pushed out. The jam wave occurs just the same, but it mostly pushes resistant cells, and since the cavity is already taken over by them, the fraction they represent inside the cavity does not change.

In the following section, we shall make some final remarks regarding the phenomenon of takeover by logistic growth.

4.4.3 Final remarks on Logistic takeover

So far, the only aspect of the logistic growth that we have not covered in the experimental curves is the actual value of the difference in growth rate, b_r , between the antibiotic-resistant and susceptible strains resulting from the fitting process, once artifacts are corrected for. The values are summarized in Table 4.1. In their experimental work in [5], the authors measure a growth rate for the microbes, in absence of antibiotic, of $0.33 \pm 0.01h^{-1}$. Although the values in Table 4.1 are not perfectly consistent with the experimental

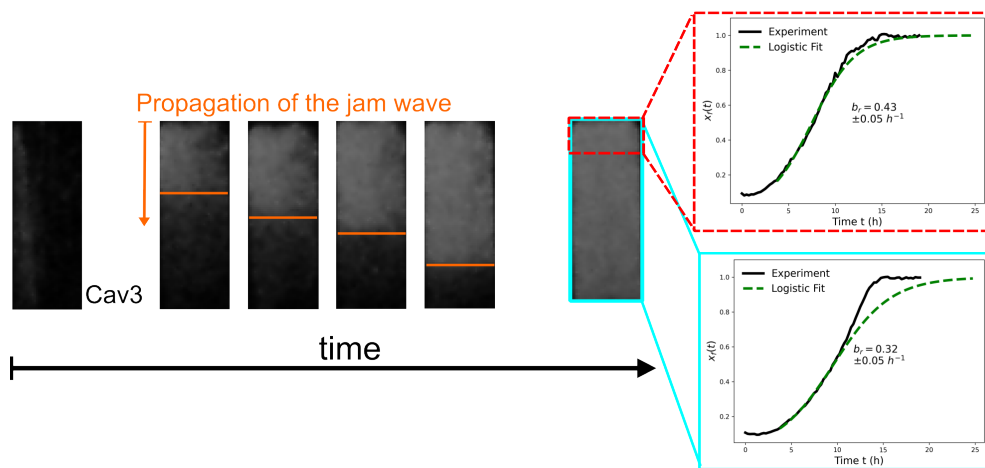


Figure 4.12: Analysis of the jam wave during takeover of the cavity by the antibiotic-resistant strain. *Left:* Snapshots of the takeover process in the cavity “Cav3”, as labeled in Figure 4.9. The approximate front of the jamming wave is pictured in orange. The two alternatives for the growth analysis, taking the entire cavity or the region near the floor, marked in cyan and red, respectively. *Right:* Growth curves for the fraction, $x_f(t)$, of antibiotic resistant (fluorescent) cells in the cavity. When the effect of the jam wave is minimized by considering only the region near the floor, takeover dynamics follow the expected logistic curve (red) and do not show the artifact resulting from the jam wave (cyan).

value from [5], they are of the correct order of magnitude, a positive outcome given how crude the image analysis of the cavities is. On top of that, the experimental value from [5] was taken in different experimental conditions from the ones analyzed here, such that the actual value might differ.

Also, conversations with Dr. Yuya Karita (who performed both the experiments in [5] and the ones analyzed here) indicated that there might be variation in birth rates across different panflutes. That is, that the levels of antibiotic that reach two cavities within a panflute will be the same, but these will be different in two different panflutes. Such a hypothesis is compatible with the results from Table 4.1, since the values of b_r are significantly closer within a panflute than across different panflutes. Still, further analyses of experimental data and possibly further experiments would be needed to determine with greater precision both the natural growth rate of the microbes

	PT	CT	Cav3	Cav4	Cav5	Cav6
$b_r \pm 0.05 (h^{-1})$	0.39	0.41	0.43	0.49	0.32	0.30

Table 4.1: Estimations of b_r from the fits to the logistic growth curve, for the different analyzed cavities. Cavities from different panflutes are separated by a double vertical line, with two cavities per panflute. The error is an estimation.

in the cavities as well as the growth rates in the presence of antibiotic.

Chapter 5

Population Distributions in Cave-like Environments

In previous chapters, we studied the spatial dynamics of microbial populations in cavities and how living in a crowded environment shapes the population inside the cavity. We also explored coexistence in a simple environment, for two strains, where one has a significant selective advantage over the other.

This sets the stage for more complex situations. After all, the population in a cavity is made up of hundreds - even thousands - of cells, and the “Who wins?” question becomes a much more complex one to answer. In particular, mutations regularly introduce new lineages in a population. These might go extinct in a short time, or grow to take up a significant fraction of the population, even fixating. One can therefore ask questions like how many clonal individuals an original ancestor will produce in a population, or what fraction a given lineage might occupy of the total population. The answers to these questions can be highly dependent on the system being studied [12, 33–39]. In this chapter, we will explore these questions for cavity-like systems, both in the jammed and in the gaseous regime.

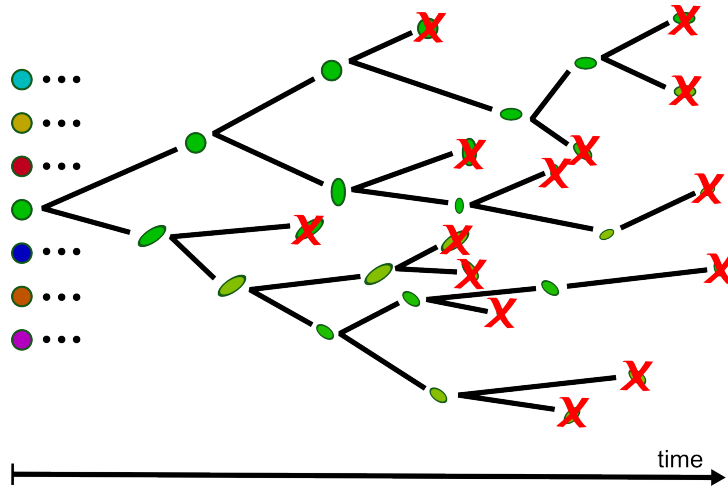


Figure 5.1: Schematics for measuring the clone size. For a given initial individual (green circle), the clone size is the total number of direct descendants from it (the total number of red crosses).

5.1 Clone-Size Distribution

In this section, we shall consider the Clone-Size Distribution (CSD) of a population in a cavity-like environment. The word “clone” in the context of population genetics refers to the group of individuals sharing the same genetic material with a common ancestor, i.e.: all of the direct descendants from that common ancestor. The word “size” refers to the total number of individuals in the clone. In a growing population where death is negligible, the CSD might refer to the number of individuals from a lineage at a given time, whereas in a population of constant size, where individuals can die, the CSD can be used to speak about the total number of individuals that ever existed from a given lineage. In both cases, measuring the clone size amounts to counting the total number of distinct individuals from a given lineage in a population (see Figure 5.1 for schematics). In the context of cavities the CSD is better understood in the second sense, as the total population in the cave is more or less constant (apart from fluctuations) and individuals and entire lineages are continuously pushed out of the cavity.

In many situations, the CSD follows a power law, such that the probability

that a clone has size n is of the form

$$P(n) \sim \frac{1}{n^\alpha} \quad (5.1)$$

where α is the characteristic exponent of the power law. For example, for an initial mutant growing exponentially within an exponentially-growing population, the CSD is known to follow a power-law with exponent $\alpha = 2$ [35, 38, 39].

It follows from Equation 5.1 that the cumulative CSD, that is the probability that a clone has size equal or larger than n , follows a power-law of the type

$$P(\text{clone size} \geq n) \sim \frac{1}{n^{\alpha-1}} \quad (5.2)$$

Throughout the rest of the manuscript, we shall often consider the cumulative CSD (as in Equation 5.2), particularly in figures.

For microbial populations in cavities, we will have to distinguish jammed and gaseous cavities.

5.1.1 Jammed cavities

Understanding the CSD in jammed cavities is motivated by the unique dynamics induced by the jamming transition. As we saw in Section 4.1, populations in jammed cavities are dominated by a few lucky cells living at the floor of the cavity, whose offspring continuously pushes out all the other cells from the cavity. We shall in the rest of this section, refer to these few lucky cells as “surfers” and to cells in the bulk as “non-surfers”. The reason will become apparent later on.

In a jammed cavity, the time taken for a non-surfing cell to be pushed out at the mouth is essentially a deterministic process. Imagine a cell initially at a distance $d(t=0) = \lambda$ from the floor of a jammed cavity of length L . Let all cells in the cavity have birth rate b . After a time $\tau = 1/b$, on average, all the cells in the cavity will have reproduced. In particular that will be true for all cells between the floor of the cavity and our marked cell. Our cell will thus find itself, at time τ , a distance $d(\tau) = 2\lambda$ away from the floor because all the cells behind it will have also reproduced. Furthermore, it will have given birth to a new cell, such that its lineage will have size 2. After a

second reproductive cycle τ , using the same argument, the original cell will find itself at distance $d(2\tau) = 4\lambda$ from the floor, and have a clone size of 4 (since both itself and the first daughter gave birth). The general trend is thus

$$d(t) = k\lambda \Rightarrow \text{Clone Size} = k \quad (5.3)$$

and so the total clone size will be given by determined by when the mother cell arrives at the mouth of the cavity, or equivalently, how many times we can divide the total length of the cavity into the cell's initial position:

$$\text{Clone Size} \equiv n = \frac{L}{\lambda} \quad (5.4)$$

where we assume that we can talk about the original mother cell or the entire lineage indistinctly since they all move in unison and will leave the cavity at around the same time. The probability that a cell yields a clone size larger than n is thus the probability that it was born a distance smaller than λ from the floor of the cavity

$$\begin{aligned} P(\text{Clone Size} \geq n) &= P(\text{initial dist. from floor} < \lambda) \sim \frac{\lambda}{L} \\ &= \frac{1}{n} \end{aligned} \quad (5.5)$$

from which it follows that the CSD is

$$P(n) \sim \frac{1}{n^2} \quad (5.6)$$

a power-law with exponent $\alpha = 2$.

Surfer cells, originally at the floor of the cavity, on the other hand, are expected to yield much larger clones, since they will keep producing new offspring for as long as they or any of their direct descendants remain at the floor. Only when the entire lineage is detached from the floor will it be doomed to extinction, by which time the number of produced offspring can be orders of magnitude higher than for a non-surfing cell. Figure 5.2.B shows the resulting cumulative CSD for a jammed cavity, distinguishing surfers from non surfers. The trend $\sim 1/n$ is also plotted, showing the agreement with the argument made above.

Remarkably, the argument used above applies to a completely different cellular system. It was in fact first introduced by the authors of [12] to

explain the CSD of cells at the front of expanding populations. For a jammed population of microbes expanding in space (where the jamming might occur due to factors other than spatial constrictions, like stickiness between cells in a biofilm), individuals can grow and reproduce for as long as they have access to nutrients. A simple situation is to assume that they can access nutrients if they are within a distance L of the expanding edge. One can thus define the expansion front of the population as the region less than L away from the expanding edge. Any cell in the expansion front will eventually be pushed away from it by the cells proliferating in front of it, following the argument made before and yielding a CSD with exponent $\alpha = 2$ as in Equation 5.6. On the other hand, a few lucky cells at the edge of the expansion front will create a lineage that “surfs” along the edge of the front (hence the term “surfers”) and yield a very large clone, much like the cells living at the floor of a cavity. For comparison with the cavity systems (Figure 5.2.B), the results from [12] are shown in Figure 5.2.A.

5.1.2 Gas Cavities

Having studied the CSD for a jammed cavity, the natural extension is to now study the case of a population in a gaseous phase.

The kind of argument used in the previous section to arrive to the CSD does not work for a gas population. The self-diffusion of the microbes is comparable to their collective diffusion, and thus movement is not approximately deterministic: a lucky cell near the mouth of the cavity might drift back into the floor and proliferate, whereas a very unlucky cell initially at the floor of the cavity can drift out of the cavity before it had the chance to have offspring.

Another question at hand is whether there is any kind of universality for gas caves the same way that there is for jammed ones. In a jammed cave, the CSD (see Equation 5.6) is independent of the length of the cavity. In previous chapters we saw that most of the dynamics in a cavity with respect to cell movement were given by the reduced length

$$l = \frac{L}{L_{est}} = \frac{2L}{\pi} \sqrt{\frac{b}{D_0}}$$

as first introduced in Equation 2.14. For the study of the CSD, on the other

hand, it is not a given that the reduced length will be enough. In particular, imagine two gaseous caves with the same reduced length but where one is much longer than the other (therefore microbes in the shorter cavity have a much larger birth rate). For instance, since the diffusion dynamics are the same in both, then a cell born some distance away from the mouth in the short cavity has a much better chance of producing offspring (because it has a larger birth rate) before being out-washed than an equivalent cell in the longer cavity

To explore the possible effects of such differences, we simulated two gas cavities at the same reduced length, one four times longer than the other ($L = 200$ vs $L = 50$ in system units). We shall discuss two similar approaches (and comment briefly on a third one) to predicting the CSD. We shall first discuss the different models and then conclude by comparing their predictions to the empirical distributions found in the simulations.

The unbiased Random Walk with a constant diffusion coefficient

The first approach is to assume that the probability, $P(n|x)$, that a cell yields a total clone size n from an initial position x with respect to the mouth of the cavity follows a master equation given by

$$\begin{aligned}
 P(n|x) = & \left[\frac{1}{2}P(n|x + \Delta x) + \frac{1}{2}P(n|x - \Delta x) \right] (1 - b\Delta t) \\
 & + b\Delta t \sum_{k=1}^{n-1} P(n-k|x)P(k|x)
 \end{aligned} \tag{5.7}$$

where b is the cell's birth rate, and Δt and Δx are the discretized time and space steps, respectively. The first term in the equation marks the probability that a cell does not reproduce in a given time step, that instead it moves one position closer or away from the mouth, then yields a clone size n . The second term represents all possible combinations in which a cell gives birth in the current time step, such that the sum of the clone sizes of it and its daughter add up to $n - 1$ (since the daughter already counts towards the clone size). Note also that we completely ignore cell movement in the direction perpendicular to the length of the cavity.

The boundary conditions for Equation 5.7 are

$$\begin{aligned} P(1|0) = 1, \quad P(n|0) = 0 \quad \forall n > 1 \\ \partial_x P(n|x)|_L = 0, \quad \forall n \end{aligned} \quad (5.8)$$

where L is the length of the cavity. The first condition relates to the fact that a cell is considered “dead” to all effects if it leaves the cave: if a cell is exactly at the mouth of the cavity, then it exits the cavity without any offspring and can thus only produce a clone size of 1 (itself and no children). Strictly speaking the cell would have to be at position $x = -\epsilon$, $\epsilon > 0$ to be considered out of the cavity, but we can simply take the $\epsilon \rightarrow 0$ limit. The second condition means that there is no flux of probability across the floor for the cavity.

In the continuous limit, Equation 5.7 can be rewritten as

$$0 = -P(n|x) + \frac{D}{b} \partial_x^2 P(n|x) + \sum_{k=1}^{n-1} P(n-k|x)P(k|x) \quad (5.9)$$

where D is a diffusion coefficient defined as

$$D = \lim_{\Delta x, \Delta t \rightarrow 0} \frac{\Delta x^2}{2\Delta t} \quad (5.10)$$

Since the random walk presented here and the physical movement of the cells in the system must obviously be related, the diffusion coefficient must in some way relate to the self-diffusion of the cells used in the simulations of the individual-based model. Since here we assume D to be a constant, we will use the value of the self-diffusion at 0 cell density, $D_0 = 1$, which coincides with the collective diffusion (see Figure 3.4 in Section 3.2 for a deeper discussion on the subject).

To find the CSD, we must only solve Equation 5.9 for increasing n and then integrate over the normalized density profile

$$P(n) = \int_{x=0}^{x=L} P(n|x) \frac{\rho(x)}{Z} dx \quad (5.11)$$

where $Z = \int_{x=0}^{x=L} \rho(x) dx$ is the corresponding normalization factor and, since the population is in a gaseous state, we assume the density profile to be well-approximated by a sine function[5]

$$\rho(x) = \rho_0 \sin\left(\frac{\pi x}{2L}\right) \quad (5.12)$$

as discussed in Section 2.1 (note the profile is now a sine instead of a cosine because we measure position from the mouth of the cavity, not the floor), with ρ_0 the value of the density at the floor of the cavity.

The special case where a cell yields a clone of total size 1 (i.e.: it does not reproduce) poses a simpler question than that of the entire CSD, and treating it separately can help us gain an intuition on the dynamics inside the cavity.

In particular, one can imagine that a cell that exits the cavity without children is likely to have performed a very unlucky random walk, with most steps falling in the direction of the mouth of the cavity and where the cell did not reproduce at any of those steps. If the reproduction event at each of those steps follows a Bernoulli distribution with probability of success equal to $b\Delta t$, then the probability that a cell did not reproduce in any of the N steps it took to exit the cavity is given by a binomial distribution

$$P(n = 1|N \text{ steps}) = (1 - b\Delta t)^N \quad (5.13)$$

Assuming that the number of steps N is large, one can imagine that the initial position of the cell with respect to the mouth of the cavity, x , can be approximately described by the root-mean-squared distance of an unbiased random walk

$$x^2 \approx 2DN\Delta t \quad (5.14)$$

Introducing Equation 5.14 into 5.13 one finds that the probability of yielding a clone sized 1 given an initial position x is given by

$$\begin{aligned} P(n = 1|x) &\approx (1 - b\Delta t)^{\frac{x^2}{2D\Delta t}} \\ &= (1 - b\Delta t)^{\frac{1}{-b\Delta t} \frac{-bx^2}{2D}} \\ &\approx e^{\frac{-bx^2}{2D}} \end{aligned} \quad (5.15)$$

where we approximated the Bernoulli distribution with an exponential one in the last step due to the fact that $b\Delta t \ll 1$.

Alternatively, one can try to work directly with Equation 5.9. The case for size-1 clones can be treated analytically, since then the summation term

in Equation 5.9 vanishes and the equation can be solved, yielding

$$P(n = 1|x) = \frac{\cosh\left(\sqrt{\frac{b}{D}}(x - L)\right)}{\cosh\left(\sqrt{\frac{b}{D}} \cdot L\right)} \quad (5.16)$$

From the simulations, we can easily obtain the distribution of initial positions of the cells with clone size 1, that is, $P(x|n = 1)$. To compare the results from Equations 5.15 and 5.16 with the empirical distribution, we can make use of the properties of conditional probabilities, from which

$$P(x|n = 1) = P(n = 1|x) \cdot \frac{\rho(x)}{Z} \cdot \frac{1}{P(n = 1)} \quad (5.17)$$

where $\rho(x)$ is the cosine profile from Equation 5.12 and Z its normalization constant, as described in 5.11. $P(n = 1)$ is estimated simply as the number of clones with size 1 divided by the initial number of cells in the simulation.

The comparison of the model predictions with the empirical distribution from simulations is found in Figure 5.3, both for a short cavity (Figure 5.3.A) and a long cavity (Figure 5.3.B). Notice how, although the exponential approximation yields an overall distribution that resembles the empirical one, the hyperbolic cosine solution of the random walk does a better job at capturing the empirical distribution, in particular its flatness close to the floor of the cavity, a phenomenon which is much more apparent for the longer cavity.

Inputting the solution for $P(1|x)$ from Equation 5.16 into Equation 5.9, we can iteratively obtain the solutions distributions for larger clone sizes, $P(n|x)$ and obtain the CSD using Equation 5.11. Although one could, in theory, obtain some of the $P(n|x)$ analytically from $P(1|x)$, doing so becomes extremely impractical and difficult beyond $n = 2$ (and even for $n = 2$ it requires a certain degree of self-hatred to obtain all the terms by hand). In practice, it is enough to solve the problem numerically to calculate the $P(n)$, which we have done using Mathematica [40]. The resulting CSD is shown in Figure 5.4, along with results from the other approaches and the empirical distribution for both the long and short cavities.

The biased Random Walk with density-dependent diffusivities

The second approach to the CSD is an extension of the unbiased random walk. Since the cells in the cavity do, in principle, feel density gradients, it seems natural to modify Equation 5.7 to make the random walk biased:

$$P(n|x) = \left[qP(n|x+\Delta x) + (1-q)P(n|x-\Delta x) \right] (1-b\Delta t) + b\Delta t \sum_{k=1}^{n-1} P(n-k|x)P(k|x) \quad (5.18)$$

where q is the parameter that controls the bias. Again, taking the continuous limit leads to

$$0 = -P(n|x) + \frac{v(\rho)}{b} \partial_x P(n|x) + \frac{D(\rho)}{b} \partial_x^2 P(n|x) + \sum_{k=1}^{n-1} P(n-k|x)P(k|x) \quad (5.19)$$

where the diffusion coefficient is given by

$$D(\rho) = \lim_{\Delta x, \Delta t \rightarrow 0} \frac{\Delta x^2}{2\Delta t} \quad (5.20)$$

and the drift term by

$$v(\rho) = \lim_{\Delta x, \Delta t \rightarrow 0} \frac{-(1-2q)\Delta x}{\Delta t} \quad (5.21)$$

and in both cases we have generalized their form to be density-dependent. In fact, using the same arguments as in the unbiased model, that the diffusion coefficient and the drift term should be related to the movement in space of the cells in the individual-based model, the natural approach is to let $D(\rho) \equiv D_s(\rho)$ the self-diffusion shown in Figure 3.4 and the drift term to be given by $v(\rho) \equiv v_{drift}(\rho) = (D_s(\rho) - D_c(\rho))\nabla \ln(\rho) + \nabla D_s(\rho)$ from the Langevin equation in the individual-based model (see Equation 3.7).

Once again, the CSD can be found by first finding $P(1|x)$, then obtaining the distributions for higher n iteratively from equation 5.19, and finally using Equation 5.11 to obtain the $P(n)$. The resulting CSD is shown in Figure 5.4 along with the empirical distribution obtained from simulations.

Well-mixed model

A third possible approach is to simply consider the CSD obtained by assuming the cells in the system go through a birth-death process in a well-mixed

population. We will not do a full derivation here (see Appendix A.3 for a full derivation, all credit goes to Dr. Valentin Slepukhin for this analytical result). In this approach, the CSD is given by

$$P(n) = \frac{1}{2} \cdot \left(\frac{1}{4}\right)^{n-1} \cdot C_{n-1} \quad (5.22)$$

where C_k is the k -th Catalan number (any similarity with the author's home region is purely coincidental). The reason Catalan numbers show up at all has to do with the form of the recursion that connects $P(n)$ for a given n with all the $P(k)$ with $k < n$ (see Equation 5 in [41]).

The resulting distribution is shown in Figure 5.4, along with the previous models and the empirical distribution from simulations, for both a long and a short cavity.

Comparison with Simulations

Figure 5.4 shows the empirical CSD obtained from simulations, as well as the predictions obtained from the three models discussed in the previous pages, both for a long ($L = 200$ in system units) and a short ($L = 50$ in system units) gas cavities.

Although all three models predict similar clone size distributions for a very small number of clones, they diverge with respect to each other as n increases. In particular, the model for the unbiased RW tends to overestimate large clone sizes with respect to the empirical distribution and the other two models, indicating that the density-dependence is a necessary introduction to the model. Still, the behavior of the two cavities seems to be distinctively different. The CSD in the long cavity (Figure 5.4.B) follows almost to perfection the prediction by the model of the biased random walk. On the other hand, the CSD in the short cavity (Figure 5.4.A) initially drops off like the prediction of the unbiased random walk and then starts dropping off faster, approaching the well-mixed prediction. It is hard to point out, exactly, what causes the difference in behavior, or if it is caused by physical phenomena at all or is simply due to uncertainty.

Although the empirical measurements of the CSD were both made when some lineages were still extant in the cavities, in all cases these remaining

lineages had clone sizes larger than the maximum clone size shown (200 individuals), so they would only add to the tail of the distribution and should not affect the interval of the CSD shown in the figures.

In any case, both the predictions and the empirical distributions indicate that the cumulative CSD drops off slower than the $1/n$ law, whereas the CSD for jammed cavities initially drops like $1/n$ and then is even steeper, until the contribution of surfer cells becomes significant. The fact that clones in gaseous cavities are of larger size indicates greater diversity than in jammed ones, where non-surfer lineages are killed fast, leading to a lower overall number of strains, consistently with the observation that the population in jammed cavities is almost exclusively driven by the lineages present at the floor of the cavity.

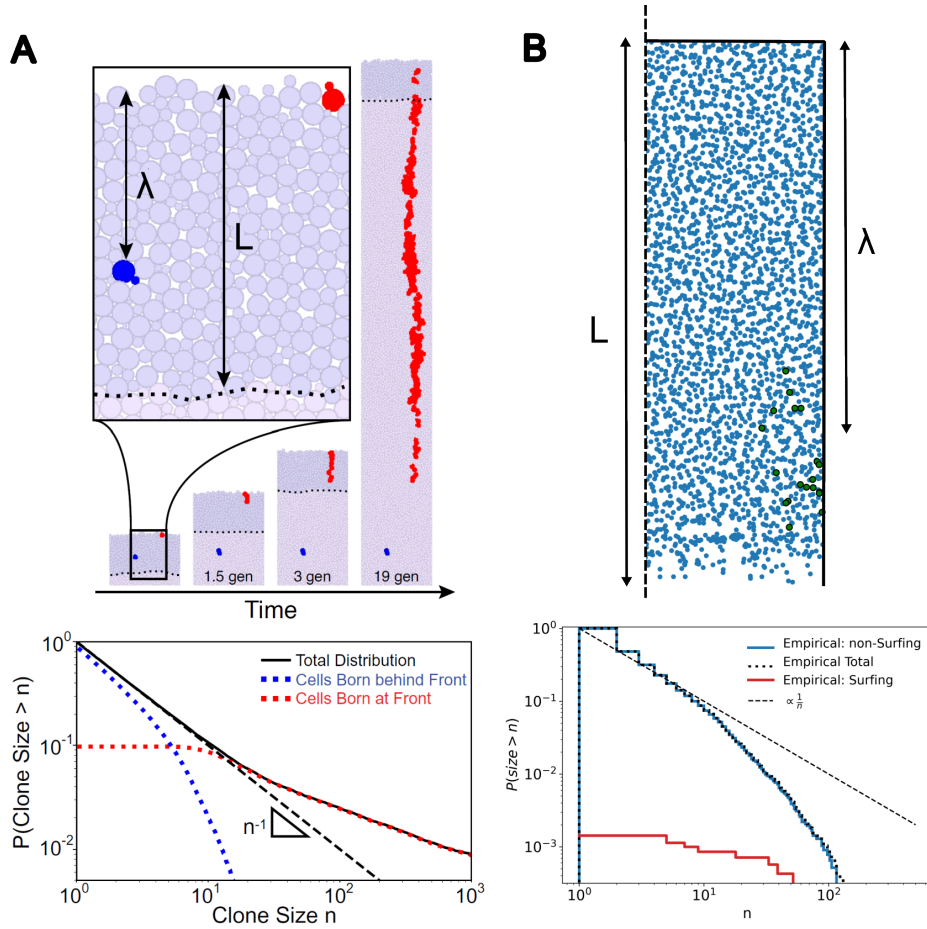


Figure 5.2: Similar cumulative CSD for two different systems. L is the total length of the expanding front in A (the jammed cavity in B) and λ the distance from the edge of the expanding front in A (distance from the floor of the cavity in B) **A)** *Modified from [12]* Simulation of an expanding population (top) and the corresponding cumulative CSD (bottom). Non-surfers at the expanding front follow the CSD described by Equation 5.5 in the main text, whereas surfers follow a slower-decreasing power-law. **B)** Part of a simulated jammed cavity (top) and the corresponding cumulative CSD (bottom). A non-surfing clone is highlighted in green. The distribution is comparable to that of A. The lower presence of surfers with respect to A has two causes: non-sampling of extant surfing lineages and a larger jammed phase with respect to the nominal cell diameter.

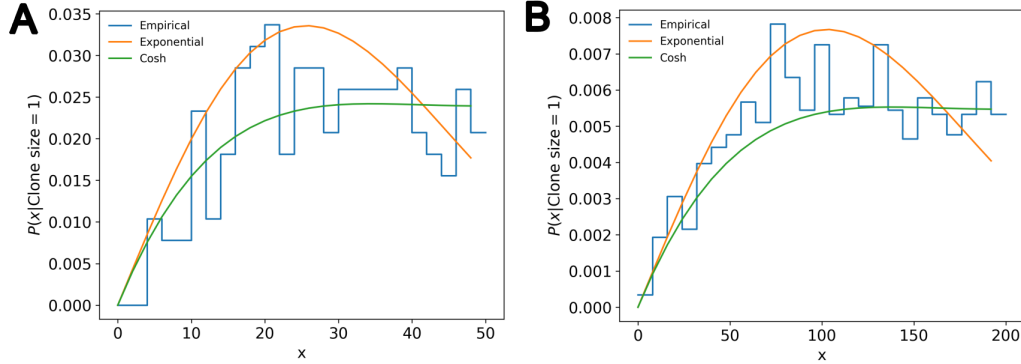


Figure 5.3: Distribution of initial positions, with respect to the mouth of the cavity, of cells with a clone size of 1. The empirical distribution obtained in simulations is shown in blue. The results obtained, using Equation 5.17, of the exponential approximation (Equation 5.15) and the hyperbolic cosine solution of the unbiased random walk (Equation 5.16) are shown in orange and green, respectively. **A)** Distribution for a short cavity ($L = 50$ system units). **B)** Distribution for along cavity ($L = 200$ system units).

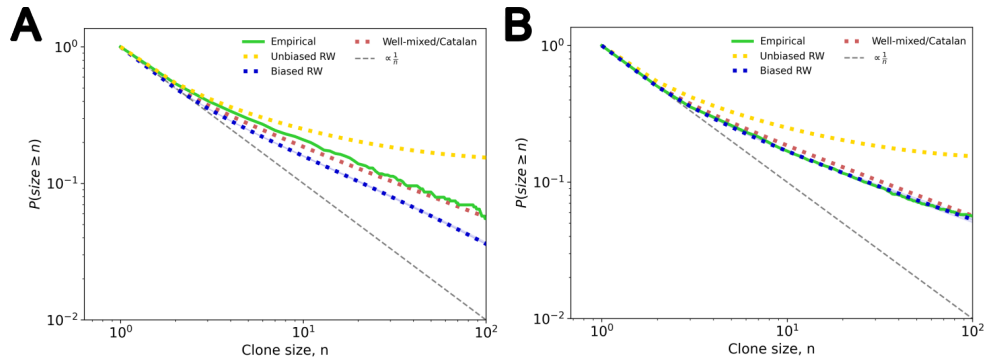


Figure 5.4: Cumulative CSD for gaseous cavities. The models discussed in the text are shown in dashed, colored lines (yellow for the unbiased random walk, brown for the well-mixed model and dark blue for the biased random walk with density-dependence). Grey dashed line shows the $1/n$ trend for reference. The empirical distribution is shown in solid green. **A)** Short gaseous cavity ($L = 50$ units). **B)** Long gaseous cavity ($L = 200$ units)

Chapter 6

Invasion and Fixation in Cave-like Environments

So far in this thesis, the only way in which we have considered coexistence of different strains was in the very-specific environment of bands in jammed cavities, in which we studied their dynamics both in the neutral case and in the case of a very strong advantage by one of the two strains, representing the addition of an antibiotic in the system. We also saw, back in Chapter 2, how a non-zero density of cells at the mouth of the cavity can populate a system that would otherwise be empty and even jam it, a hypothesis that we qualitatively tested in Section 3.1. In this chapter, we shall investigate this Outsider-Induced Population (OIP) of cavities in a quantitative manner. We shall also study one of its consequences, the almost paradoxical Invader-Sustained Jamming (ISJ), introduced also in Chapter 2, whereby an outsider population of invading cells is capable of stabilizing a resident population in a jammed state.

The second part of the chapter will be dedicated to invasion and fixation processes in gaseous cavities, that is, the study of the fate of an initial mutant appearing somewhere in the cavity as a function of its position and its selective advantage with respect to the rest of the cells in the cavity.

6.1 Outsider-Induced Population

Back in Section 2.4, we discussed the effects of having a non-zero density of cells at the mouth of the cavity, which can produce a population inside the cavity that can be either in the gas or the jammed state (the OIP). We saw that the one-dimensional reaction diffusion system discussed in Section 2 could be used to make quantitative predictions for the density of cells at the floor of the cavity as a function of the density of cells at the mouth and could be used to plot the corresponding bifurcation diagram for the establishment and the gas-jam transition (see Figure 2.9 in Chapter 2).

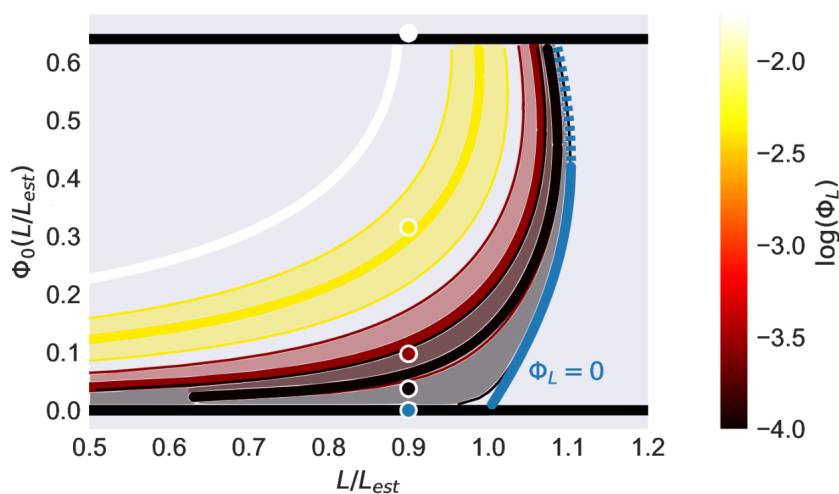


Figure 6.1: Test of Outsider-Induced Population (OIJ). Bifurcation diagram, similar to those shown in Chapter 2, with the expected packing fraction at the floor of the cavity, Φ_0 , as a function of the reduced length of the cavity, for different values of the packing fraction at the mouth of the cavity, Φ_L (the colormap is in logarithmic scale for better color visualization). The colored dots are the result of simulations of cavities using the individual-based model to test the hypothesis of OIJ. The colored curves are the expected bifurcation diagrams for the Φ_L from the simulations (shaded regions indicate one standard deviation from the measured Φ_L value in the individual-based simulations).

In Chapter 3, we introduced a soft disk model that could be used to qual-

itatively test OIP (see Section 3.1). Here, we use the individual-based model with two diffusivities introduced in Section 3.2 to test OIP in a quantitative manner.

Figure 6.1 shows the value of the packing fraction expected at the floor of the cavity as a function of the reduced length of the cavity and the packing fraction of cells at the mouth. The colored dots are the results of numerical simulations for different values of packing fractions at the mouth. We can see that agreement is good between the predictions of the 1D reaction-diffusion model and the 2D individual-based model, despite their very different nature.

This result mainly serves to check that the two models agree with each other, and thus the 1D reaction-diffusion model can be reliably used to set the desired behavior in the 2D individual-based model.

6.2 Invader-Sustained Jamming

One natural consequence of OIP, as discussed in Section 2.4, is the phenomenon of Invader-Sustained Jamming (ISJ), whereby a population of invader cells can sustain the resident population of a cavity in a jammed state such that the jamming prevents the invader itself from taking over. In this section, we show that ISJ occurs, not only for the case of neutral competition, but also if the invader has a significant selection advantage.

Let b be the birth rate of a given cell. Another cell is said to have a selective advantage s if its birth rate is $b_s = b \cdot (1 + s)$. Figure 6.2 shows snapshots of simulations showing ISJ, for invading populations with different selective advantages, from the neutral case, $s = 0$, to a very high selective advantage, $s = 5$. In all cases, the invader strain is unable to invade the cavity in the duration of the simulation. In fact, the strain is barely able to penetrate into the jammed phase of the resident strain. This showcases just how resilient a jammed population is, even in the presence of an ecological adversary whose fitness is huge in comparison. For context, when studying the takeover of a cavity presenting bands by an antibiotic resistant strain, the resistant strain had a selective advantage $s = 0.43$ and the dynamics in the cavity were essentially deterministic, with it taking over the entire system. In contrast, a strain with a selective advantage an order of magnitude larger

can barely scratch the surface of a jammed population when invading from outside. One wonders if, in the context of populations of cavities, the well known “survival of the fittest” could appropriately be replaced by “survival of the jammed”, such is the power of jamming.

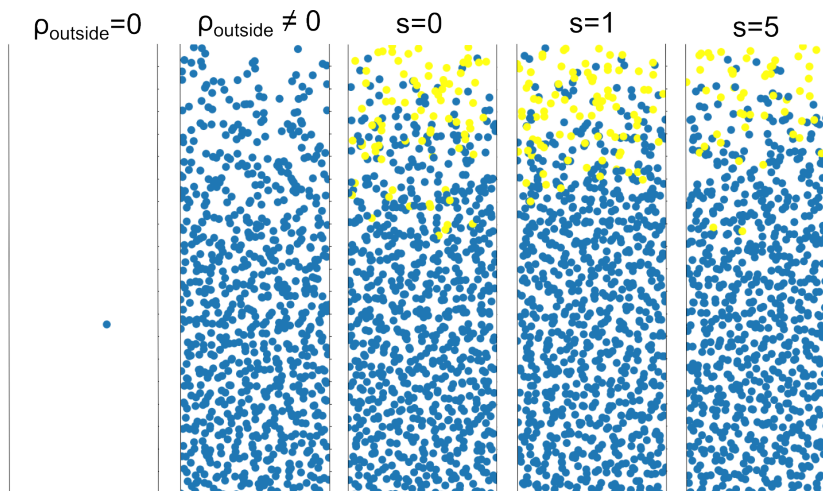


Figure 6.2: Invader Sustained Jamming. The resident strain is shown in blue, the invader in yellow. The figure shows snapshots of a cavity under various conditions. If the density of cells at the mouth of the cavity is set to 0, the cavity eventually empties out (first from left). If it is non-zero, then the outsider population can populate the cavity and even bring it to a jammed state (second from left). If the outsider population changes from the resident strain to an invader, then the invader sustains the resident population in the jammed state without being able itself to invade the cavity, and this is so for a large range of selective advantages (three rightmost cavities). s is the relative selective advantage of the invader, with $b_{\text{invader}} = b_{\text{resident}}(1 + s)$

While altruism and cooperation are not rare in biology [42], there is usually some mutual benefit for the parties involved, and so perhaps the most surprising thing of ISJ is that the invader gains absolutely nothing from the interaction. And we should recall that without its presence the population of resident cells would not even stably exist!

ISJ has potential consequences at different scales. In the context of disease control, for example, it might allow a pathogen in the intestine to remain “hidden” at the bottom of cavities, when put under the influence of antibi-

otic, by another microbial strain that is native to the gut and resistant to the antibiotic. In the context of evolution, on the other hand, ISJ could potentially imply a decrease in the speed of evolution, since it allows very underfit strains to survive in an environment for long periods of time. Or maybe it can be seen as a potential source of diversification, since it might allow a large number of unfit populations to remain blocked at the floor of cavities, ready to blossom if the conditions outside the cavities suddenly change.

Chapter 7

Discussion

In this section, we shall discuss in more detail the results presented throughout the thesis, discussing also their relevance to the topic of island biogeography and presenting potential future paths of research.

We have seen that cavity-like systems can be described using a wide array of models, from continuous models (the 1D reaction-diffusion system or the 2D reaction-diffusion system with two diffusivities) to individual-based models of different kinds (the soft-disk model and the model of point-like cells with two diffusivities).

The prediction from the one-dimensional reaction-diffusion model that resource-depletion stabilizes the gaseous phase and cooperation promotes jamming are consistent with the intuitive expectation. The apparently strong stability of microbial populations in cavity-like systems [13, 14, 19] indicates that jamming is likely prevalent in real systems [14]. This could indicate that resource depletion is negligible in real cavities. After all, in the idealized case of hard spheres there is still around 36% of empty space in the jammed phase, and even if real cells differ from the hard sphere assumption (which they certainly do), either by differences in shape or in squishiness (thus allowing cells to compact closer together), one might expect that there is still enough space for nutrients to flow along the cavity. Most likely, though, especially if nutrients only enter the cavity from the mouth, resource depletion will be significant closer to the floor of the cavity as it gets used up by cells near the mouth. In that case, even if resource depletion is very strong, one might

still expect to find jammed cavities as long as the region near the mouth where resource-depletion is weak is long enough for jamming to occur. In that scenario, one might find that the region near the bottom of the cavity is filled with dead or frozen (non-proliferating) cells. In our model we have neglected any spatial dependence of the logistic effect, and one possible area of future research would be to study such spatial dependence.

Regarding the Allee effect, we have seen that it can act as a potential stabilizer of the jammed phase, thus contributing to the stability of populations in cavity-systems. Although it cannot cause jamming to arise (see Figure 2.6, the establishment length is independent of the Allee effect because it relies on the dynamics at zero-density) it can prevent gasification of cavities under adverse conditions. One aspect left untouched in this thesis is the treatment of cooperation at the individual-based level. A given microbe is expected to interact with its neighbors (directly through contact, or effectively, for example through the presence of some secreted substance). This opens up the possibility of inter-strain (even inter-species) cooperation, and the possible density profiles and spatial structures that would arise from such interactions and how they could be compatibilized with the floor-driven dynamics in jammed cavities is for now a complete unknown. Regardless, experimental results point to cavities mostly occupied by single microbial strains [14], implying that inter-strain cooperation is a rather exotic event.

The discovery of Invader-Sustained Jamming (predicted by the 1D reaction-diffusion system and confirmed in the individual-based model) as a novel cooperation effect could potentially play a significant role in shaping the ecological landscape of a system full of cavities. In particular, it can allow underperforming strains to survive in the system for long periods of time being supported by the stronger strains outside a cavity. This can have a positive effect for rediversification after extreme events, since it might allow for a pool of different microbial strains to be ready to thrive if conditions in the system change dramatically. On the other hand, it can potentially have negative consequences, as it might allow a pathogen to survive unnoticed for a long time, being ready to thrive in much the same manner. It must be noted, though, that invader-sustained jamming is studied here in the simplest of cases. Hydrodynamical interactions between cells have been completely neglected in this thesis, as well as the dynamics of the fluid around them. These could prove potentially disruptive to the stability of the jammed, underfit population, as currents might help flush out the strain inside the cavity

and allow the fitter strain to take over. In fact, the introduction of fluid dynamics in the present models would be a natural extension of the research presented here. It is known from experiments that taller cavities (properly three dimensional, larger in the dimension that we have ignored throughout this thesis) sometimes present vortices in the interior, at least in the gaseous phase. Furthermore, although advection can safely be neglected far from the mouth of the cavity under some conditions, it is generally not the case close to it [5]. It would thus seem reasonable to include advection and hydrodynamic interactions in our models and study their potential effects (applied to ISJ but also in general to other phenomena), even if this would naturally increase the computational cost of the models.

Regarding the stability of bands in jammed cavities it is important to underline the overall good agreement, between the theory and experiments, of the prediction that the fitter strain will take over the cavity via logistic growth in the absence of pinning phenomena. The relevance of this result lies in that it shows that the takeover process is, in principle, quantitatively predictable. Naturally, the result presented here is only a first step towards a more complete theory of competition processes in crowded environments. In particular, although we also show that the presence of pinning barriers prevents logistic takeover from occurring, even if only temporarily, we do not give a precise theory of how the pinning barrier might potentially be overcome (something that is observed both in simulations and experimental recordings). We also did not discuss in detail the speed of the jamming waves that sometimes occur during the takeover process. These are clear directions of future research. That is specially so with regards to the pinning, since in real systems one might expect that the kind of impurities that difficult the takeover are commonplace. If a more complete statistical theory were developed, it might open up the possibility of understanding the dynamics in systems comprising of many cavities, maybe uncovering novel phenomena.

The results in this thesis also point out some of the fundamental differences in behavior between gas and jammed cavities. In particular, the study of the Clone Size Distribution (CSD) of cavities shows the decrease in lineage size in cavities upon jamming, and points to a general loss of diversity in jammed cavities, a view that is backed up by other results of this thesis: the fact that jammed dynamics are dominated by a few cells at the floor of the cavity or the resistance to invasion conferred to the resident population by jamming being two examples. The sharp change in dynamics at the jam-

ming threshold supports the idea of Levin that scale plays a central role in ecosystem dynamics. What is more, the drop in diversity in jammed cavities directly contradicts one of the pillars of island theory, that the number of species in an ecosystem scales in proportion to the system's physical size. Our results show that an increase in system size can lead to a sudden change in system behavior that has the opposite effect to the prediction by MacArthur and Wilson. Similarly, the potential for immigration of strains into cavities is neutralized by the colonization resistance of the jammed state, even though in such a cavity the number of strains is minimum (likely to be one, maybe more if stable pinning allows it), in contradiction with island theory.

That said, we do not intend to say that the results of this thesis invalidate island theory. MacArthur and Wilson's ideas served as the breeding ground for new concepts in biology, like the r/K selection theory (the idea that some species focus on high birth rate and mortality while others have very low birth rates but in which individuals take great care of offspring to ensure they reach reproductive maturity with a high probability), or have been useful in gaining insight to problems like maintaining high diversity in the presence of the competitive exclusion principle (see [43] as an example). In fact, some of our results agree with island theory: extinction rates of lineages in the short (small) gaseous cavity were significantly higher than in the long (large) gaseous cavity, and the rate of extinction did gradually drop as the number of lineages remaining in the cavity diminished. Our other results only point out to the need to take utmost care when considering simple ecological models without much consideration. Here we only studied a very particular ecosystem, one that is surely not representative of every ecosystem in the natural world. Regardless, it is an ecosystem whose properties sometimes contradict expectations, one that points to the importance of scale in ecology.

Bibliography

- [1] Robert H. MacArthur and Edward O. Wilson. *The Theory of Island Biogeography*. Princeton University Press, 1967. ISBN: 9780691088365.
- [2] Jianguo Wu and John L. Vankat. “Island Biogeography: Theory and Applications”. In: *Encyclopedia of Environmental Biology 2* (1995), pp. 371–379.
- [3] Simon A. Levin. “The Problem of Pattern and Scale in Ecology”. In: *Ecology* 73.6 (1992), pp. 1943–1967.
- [4] Oskar Hallatschek and David R. Nelson. “Gene Surfing in Expanding Populations”. In: *Theor Popul Biol* 73.1 (2008), pp. 158–170. DOI: 10.1016/j.tpb.2007.08.008.
- [5] Yuya Karita, David T. Limmer, and Oskar Hallatschek. “Scale-dependent tipping points of microbial colonization resistance”. In: *PNAS* 119.7 (2022). DOI: <https://doi.org/10.1073/pnas.2115496119>.
- [6] Steward T.A. Pickett and John N. Thompson. “Patch dynamics and the design of nature reserves”. In: *Biology Conservation* 13 (1978), pp. 27–37.
- [7] A.J. Higgs. “Island biogeography theory and nature reserve design”. In: *Journal of Biogeography* 8 (1981), pp. 117–124.
- [8] B.L. Zimmerman and R.O. Bierregaard. “Relevance of the equilibrium theory of island biogeography and species-area relations to conservation with a case from Amazonia”. In: *Journal of Biogeography* 13 (1986), pp. 133–143.
- [9] Oskar Halatschek et al. “Genetic drift at expanding frontiers promotes gene segregation”. In: *PNAS* 104.50 (2007), pp. 19926–19930.

- [10] Oskar Halatschek and David R. Nelson. “Life at the front of an expanding population”. In: *Evolution* 64.1 (2009), pp. 193–206.
- [11] Morgan Delarue et al. “Self-driven Jamming in growing microbial populations”. In: *Nature Physics* 12 (2016), pp. 762–766. DOI: <https://doi.org/10.1038/nphys3741>.
- [12] C. F. Schreck et al. “Impact of crowding on the diversity of expanding populations.” In: *Proceedings of the National Academy of Sciences of the United States of America* e2208361120 (2023). DOI: <https://doi.org/10.1073/pnas.2208361120>.
- [13] Heidi H. Kong and Julia A. Segre. “Skin Microbiome: Looking Back to Move Forward”. In: *Journal of Investigative Dermatology* 132 (2012), pp. 933–939. DOI: <http://dx.doi.org/10.1038/jid.2011.417>.
- [14] Arolyn Conwill et al. “Anatomy promotes neutral coexistence of strains in the human skin microbiome”. In: *Cell Host Microbe* 30.2 (2022), pp. 171–182. DOI: 10.1016/j.chom.2021.12.007..
- [15] S. Melanie Lee et al. “Bacterial colonization factors control specificity and stability of the gut microbiota”. In: *Nature* 501 (2013), pp. 426–429.
- [16] Allan M. Mowat and William W. Agace. “Regional Specialization within the intestinal immune system”. In: *Nature Reviews Immunology* 14.10 (2014), pp. 667–685.
- [17] Lauriane Onfroy-Roy et al. “Extracellular Matrix Mechanical Properties and Regulation of the Intestinal Stem Cells: When Mechanics Control Fate”. In: *Cells* 9.12 (2020), p. 2629.
- [18] Nigel A.S. Taylor and Christiano A. Machado-Moreira. “Regional variations in transepidermal water loss, eccrine sweat gland density, sweat secretion rates and electrolyte composition in resting and exercising humans”. In: *Extreme Physiology and Medicine* 2.4 (2013).
- [19] Julia Oh et al. “Temporal stability of the human skin microbiome”. In: *Cell* 165.4 (2016), pp. 854–866.
- [20] Gregory P. Donaldson, S. Melanie Lee, and Sarkis K. Mazmanian. “Gut biogeography of the bacterial microbiota”. In: *Nature Reviews Microbiology* 14 (2016), pp. 20–32.

- [21] Norman F. Carnahan and Kenneth E. Starling. “Equation of State for Nonattracting Rigid Spheres”. In: 51.2 (July 1969), pp. 635–636. DOI: 10.1063/1.1672048.
- [22] G D Scott and D M Kilgour. “The density of random close packing of spheres”. In: *Journal of Physics D: Applied Physics* 2.6 (1969), p. 863. DOI: 10.1088/0022-3727/2/6/311. URL: <https://dx.doi.org/10.1088/0022-3727/2/6/311>.
- [23] Hiroshi FUJIKAWA, Akemi KAI, and Satoshi MOROZUMI. “A New Logistic Model for microbial Growth”. In: *Food Hygiene and Safety Science (Shokuhin Eiseigaku Zasshi)* 44.3 (2003), pp. 155–160. DOI: 10.3358/shokueishi.44.155.
- [24] Pierr François Verhulst. “Notice sur la loi que la populations suit dans son accroissement”. In: *Correspondence Mathematique et Physique*. X (1838).
- [25] Andrew M. Kramer, Luděk Berec, and John M. Drake. “Editorial: Allee effects in ecology and evolution”. In: *Journal of Animal Ecology* 87.1 (2018), pp. 7–10. DOI: <https://doi.org/10.1111/1365-2656.12777>. eprint: <https://besjournals.onlinelibrary.wiley.com/doi/pdf/10.1111/1365-2656.12777>. URL: <https://besjournals.onlinelibrary.wiley.com/doi/abs/10.1111/1365-2656.12777>.
- [26] RajReni B. Kaul et al. “Experimental demonstration of an Allee effect in microbial populations”. In: *Biol. Lett.* 12 (2016). DOI: <https://doi.org/10.1098/rsbl.2016.0070>.
- [27] Robert Smith et al. “Programmed Allee effect in microbia causes a tradeoff between population spread and survival”. In: *PNAS* 111.5 (2013), pp. 1969–1974. DOI: <https://doi.org/10.1073/pnas.1315954111>.
- [28] Stefan Vet, Lendert Gelens, and Didier Gonze. “Mutualistic cross-feeding in microbial systems generates bistability via an Allee effect”. In: *Scientific Reports* 10.7763 (2020). DOI: <https://doi.org/10.1038/s41598-020-63772-4>.
- [29] John D. Weeks, David Chandler, and Hans C. Andersen. “Role of Repulsive Forces in Determining the Equilibrium Structure of Simple Liquids”. In: 54.12 (June 1971), pp. 5237–5247. DOI: 10.1063/1.1674820.

- [30] Gebreselema Gebreyohannes et al. “Challenges of intervention, treatment, and antibiotic resistance of biofilm-forming microorganisms”. In: *Heliyon* 5.e02192 (2019). DOI: <https://doi.org/10.1016/j.heliyon.2019.e02192>.
- [31] César de la Fuente-Núñez et al. “microbial biofilm development as a multicellular adaptation: antibiotic resistance and new therapeutic strategies”. In: *Current Opinion in Microbiology* 16 (2013), pp. 580–589. DOI: <http://dx.doi.org/10.1016/j.mib.2013.06.013>.
- [32] M.D. Abramoff, P.J. Magalhaes, and S.J. Ram. “Image Processing with ImageJ”. In: *Biophotonics International* 11.7 (2004), pp. 36–42.
- [33] Jonathan Desponds, Thierry Mora, and Aleksandra M. Walczak. “Fluctuating fitness shapes the clone-size distribution of immune repertoires”. In: *PNAS* 113.2 (2015), pp. 274–279. DOI: <https://doi.org/10.1073/pnas.1512977112>.
- [34] Jiseon Min et al. “Spatial structure alters the site frequency spectrum produced by hitchhiking.” In: *Genetics* 222.3 (2022), iyac139. DOI: <https://doi.org/10.1093/genetics/iyac139>.
- [35] In: *Genetics* 210.3 (2018), pp. 1053–1073. DOI: <https://doi.org/10.1534/genetics.118.301516>.
- [36] Richard A. Neher and Oskar Hallatschek. “Genealogies of rapidly adapting populations”. In: *PNAS* 110.2 (2012), pp. 437–442. DOI: <https://doi.org/10.1073/pnas.1213113110>.
- [37] Ronald A. Fisher. *The Genetical Theory of Natural Selection*. Oxford University Press, 1930. ISBN: 9780198504405.
- [38] Salvador E. Luria and Max Delbrück. “Mutations of microbia from Virus Sensitivity to Virus Resistance”. In: *Genetics* 28.6 (1943), pp. 491–511. DOI: [10.1093/genetics/28.6.491](https://doi.org/10.1093/genetics/28.6.491).
- [39] George U. Yule. “A mathematical theory of evolution, based on the conclusions of Dr. J. C. Willis, F. R. S”. In: *Philosophical Transactions of The Royal Society London B* 213 (1925), pp. 21–87. DOI: <https://doi.org/10.1098/rstb.1925.0002>.
- [40] Wolfram Research Inc. *Mathematica, Version 13.2*. Champaign, IL, 2022. URL: <https://www.wolfram.com/mathematica>.

- [41] Igor Pak. “History of Catalan numbers”. In: *arXiv: History and Overview* (2014).
- [42] Tim Clutton-Brock. “Cooperation between non-kin in animal societies”. In: *Nature reviews* 462.5 (2009). DOI: 10.1038/nature08366.
- [43] Michael T. Pearce, Atish Agarwala, and Daniel S. Fisher. “Stabilization of extensive fine-scale diversity by ecologically driven spatiotemporal chaos”. In: *PNAS* 117.25 (2020), pp. 14572–14583. DOI: <https://doi.org/10.1073/pnas.1915313117>.

Appendix A

Appendix

A.1 Establishment length

This derivation follows closely that found in the Supplementary Information of [5].

Recall that the 1D reaction-diffusion system is given by

$$\begin{aligned}\partial_t \rho(y, t) &= -\partial_y(j(y, t)) + b(\rho(y, t)) \\ j(y, t) &= -D(\rho)\partial_y \rho(y, t)\end{aligned}\tag{A.1}$$

with boundary conditions

$$\begin{aligned}j(0, t) &= 0, \quad \forall t \\ \rho(L, t) &= \rho_L, \quad \forall t\end{aligned}\tag{A.2}$$

where $\rho(y, t)$ is the density at position y (with respect to the floor of the cavity) and t is the time, $D(\rho)$ is the diffusivity, j is the current of density and $b(\rho)$ the birth term due to cell proliferation.

Given the no-flux boundary conditions at the floor and zero-density boundary conditions at the mouth, it makes sense to expand the density profile as a sum of cosine modes:

$$\rho(y, t) = \sum_{n=1} a_n(t) \cos(k_n y), \quad k_n = (2n + 1) \frac{\pi}{2L}\tag{A.3}$$

where the dependence on time is in the amplitude of each mode.

Around $\rho \approx 0$, Equation A.1 then reduces to an equation for each mode. The diffusivity reduces to $D_0 \equiv D(0)$ at zero density and the birth function reduces to an exponential growth term (any effect of logistic growth or Allee is at least order $O(\rho^2)$). The equation for a given mode is then

$$\partial_t a_n(t) \cdot \cos(k_n y) = a_n(t) D_0 \cdot (-k_n^2) \cdot \cos(k_n y) + b a_n(t) \cos(k_n y) \quad (\text{A.4})$$

The cosine drops out and we are left with

$$\partial_t a_n(t) = (-D_0 k_n^2 + b) a_n(t) \quad (\text{A.5})$$

for each of the modes' amplitudes.

For each of the modes, the zero-amplitude state is unstable and the amplitude grows if $-D_0 k_n^2 + b > 0$. On the other hand, it to 0 if $-D_0 k_n^2 + b < 0$. When the empty state of the lowest mode, $n =$, changes, all higher modes still go to zero because $k_n > k_0 \forall n > 0$. The stability of the empty state is then given by this lowest mode and the empty state becomes unstable overall when

$$b = k_0^2 \cdot D_0 = \left(\frac{\pi}{2L_{est}} \right)^2 D_0 \implies L_{est} = \frac{\pi}{2} \sqrt{\frac{D_0}{b}} \quad (\text{A.6})$$

where L_{est} is thus the establishment of the cavity, and the expression corresponds to that in Equation 2.4 in the main text.

A.2 Inter-band boundary under pinning.

Let \hat{y} be the direction along the length of the cavity and \hat{x} the transversal direction, with the origin in the region of higher growth rate. The heuristic of logistic growth discussed in the main text, when applied to a point (x, y) along the boundary between two bands, leads to

$$\dot{x} \equiv \frac{dx}{dt} = b_r x(1 - x) \quad (\text{A.7})$$

in the \hat{x} -direction, where $b_r = b_{high} - b_{low}$ is the difference in growth rates between the two strains. Note that x is normalized with respect to the width of the cavity, i.e. it goes from 0 to 1.

In the \hat{y} -direction, on the other hand, the velocity of a cell (or equivalently, of a point in space) is driven by the growth of the cells behind it, beginning at the floor, and is exponential in the number of cells behind it, leading to a velocity in the \hat{y} -direction given by

$$\dot{y} \equiv \frac{dy}{dt} = b_{low}y \quad (\text{A.8})$$

where the growth rate is that of the weaker strain, since we expect that the boundary curves towards the region of the weaker strain and so the space between the boundary curve and the wall is expected to be filled with cells of the lower growth rate.

The curve of the inter-band boundary is thus described by the following equation:

$$\frac{dx}{dy} \cdot \frac{dy}{dt} = \frac{dx}{dt} \quad (\text{A.9})$$

which using the above expressions can be rewritten as

$$\frac{dx}{b_r x(1-x)} = \frac{dy}{b_{low}y} \quad (\text{A.10})$$

the solution of which is, by integration,

$$\frac{b_{low}}{b_r} \log\left(\frac{x}{1-x}\right) = \log(y(x)) + C \quad (\text{A.11})$$

which is the same result as in Equation 4.6 in the main text. The constant of integration can be set from the boundary conditions, in particular that:

$$y_0 = L_w \iff x_0 = 0.5 \quad (\text{A.12})$$

where L_w is the length of the pinning impurity.

A.3 Well-mixed approach to the CSD

Take a birth-death process where a cell reproduces with birth rate b and dies with rate d . The probability that a cell yields a clone of size n , following the same recursive approach used in the main text, is given by

$$P(n) = \frac{b}{d+b} \sum_{k=1}^{n-1} P(k) \cdot P(n-k) \quad (\text{A.13})$$

for $n > 1$. $P(n = 1)$, which is simply the probability that a cell dies without reproducing, is given by

$$P(n = 1) = \frac{d}{d+b} \cdot K_1 \quad (\text{A.14})$$

where K_1 is some arbitrary prefactor.

Looking at the first few terms, we can quickly see a recurrence relation, yielding that the probability to give a clone size of n is

$$P(n) = \frac{d}{d+b} \left(\frac{b}{d+b} \cdot \frac{d}{d+b} \right)^{n-1} K_n, \quad K_n = \sum_{i=1}^{n-1} K_i K_{n-i} \quad (\text{A.15})$$

The recursion can be mapped to the recursive expression of the Catalan numbers, using $K_n \rightarrow C_{n-1}$.

In order to have a stable steady-state population, the only possibility is that $d = b = 1/2$. This leads to

$$P(n) = 1/2 \cdot (1/4)^{n-1} \cdot C_{n-1} \quad (\text{A.16})$$

as in the main text.